Università
Ca'Foscari
Venezia

Corso di dottorato in ricerca in
Scienze e Gestione dei Cambiamenti Climatici
ciclo 31

TESI DI RICERCA

Impact of reduced sea ice conditions in the Barents-Kara Seas on wintertime atmospheric circulation in the Euro-Atlantic sector

SSD: GEO/12

Anne Seidenglanz
Ca' Foscari University of Venice

Coordinatore del Dottorato
Supervisori
Prof. Carlo Carraro

Dr. Panos Athanasiadis
Dr. Silvio Gualdi

Dottoranda
Anne Seidenglanz
(Matricola 956213)

Acknowledgements

This work would have been impossible without the help of my supervising team. In particular, I thank Panos Athanasiadis and Silvio Gualdi for their enduring support and help in guiding me through this challenging period in all its aspects. This work has benefited to a substantial fraction from the advice from Paolo Ruggieri regarding Arctic-mid-latitude linkages and running SPS3 on Athena. By the same token, I thank Antonella Sanna and Andrea Borrelli for their technical advice on issues related to running the model smoothly and managing the overwhelming output.

This work has benefited from my stay abroad in Bergen, Norway, in 2018 and here my thanks go to Camille Li who has hosted me during this period. Being part of and interacting with her group has deepened my understanding in Arctic-related processes and in particular Arctic-mid-latitude connections.

Abstract

Despite the globally-averaged warming trend over the recent decades, there have been several severe cold winter spells over northern Eurasia. Accelerated sea-ice retreat over the Barents-Kara Seas (BKS) during early winter has been considered a leading driver of these recent mid-latitude severe winters over Eurasia. Observational and numerical model studies have increased our understanding of pathways that link late autumn sea ice loss in the Barents-Kara Seas to atmospheric circulation anomalies over the Euro-Atlantic sector in late winter, but yet, observational analysis give us clear limitations in inferring Arctic-mid-latitude linkages and model studies generally do not agree on the timing and character of the response, indicating that the response is to some extent model-dependent.

This study presents results from idealized sensitivity experiments with reduced sea ice conditions in the BKS during late autumn (November) using a fully-coupled operational seasonal prediction system. Initialized forecast simulations that represent realistic winter seasons of the recent hindcast period (1993-2015) with a well-resolved stratosphere in the atmospheric model component sets this study apart from earlier studies. The experimental set-up allows for taking into account inter-annual variability associated with planetary-scale teleconnections. Additionally, the procedure followed represents a noval way to implement sea ice-free conditions in an ocean model in a coupled model framework. Results indicate an initial, fast, thermodynamic response over the imposed heating area (November, December) which translates into larger-scale circulation anomalies with the progress of the winter season. By January, sea level pressure and geopotential height anomalies imply a deep, equivalent barotropic circulation response that resembles the positive phase of the North Atlantic Oscillation (NAO). This latter, rather unexpected result is suggested to be due to a positive bias in the simulated eddy-driven jet stream intensity over the Euro-Atlantic sector which has previously shown to cause a switch from a negative NAO-like to a positive NAO-like circulation response in a coupled model study. This finding stresses again the significance of state- or model dependence when studying Arctic-mid-latitude linkages.

These results invite for a deeper analysis of the response, such as the previously demonstrated linear interference with the climatological wave pattern and changes in the position and intensity of the North Atlantic storm track.

Table of Contents

Acronyms and Abbreviations

BKS - Barents-Kara Seas

SIC - Sea ice concentration

ENSO - El Niño Southern Oscillation

SPS - Seasonal Prediction System

CMCC - Euro-Mediterranean Centre of Climate Change

NSIDC - National Snow and Ice Data Center

AGCM - Atmospheric General Circulation Model

NAO - North Atlantic Oscillation

AO - Arctic Oscillation

NH - Northern Hemisphere

ITCZ - Intertropical convergence zone

SHF - Surface heat fluxes

THF - Turbulent heat fluxes

WACS - Warm Arctic - Cold Siberian Pattern

1. Introduction

1.1 Recent trends in northern hemisphere climate

The Arctic cryosphere has undergone rapid changes in the recent decades. At the same time, the high latitudes have been warming at a rate that exceeds the global average by a factor of more than two (2°C warming since 1990) over the last decades, a fact which is referred to as Arctic or Polar amplification (Cohen et al., 2014, IPCC, 2013). Arctic amplification is present in all seasons but most pronounced in autumn and winter and is a consistent feature of recent past and future climate projections that are forced with increased greenhouse gas concentrations (Holland et al., 2003). A number of processes have been suggested to act or enhance surface warming at high latitudes, one of which is the decrease in Arctic sea ice extent (Screen et al., 2010). The fact that this decline happens at an accelerating rate implies that Arctic sea ice could act as both driver and response to Arctic surface warming (Screen and Simmonds, 2010, Stroeve et al., 2012). Therefore, a number of studies have emphasized its potential profound impact on the climate and weather at lower latitudes (Cohen et al., 2014, Vihma et al., 2014, Overland et al., 2016, Screen et al., 2018, Smith et al., 2017). For example, despite the recent global average warming trend of the high latitude northern hemisphere land and oceans, there exists a spatial inhomogeneity in this warming, and the northern hemisphere continents have seen an increasing number of unusually cold winter months. One of the debates is whether features like cold extremes arise due to changes in Arctic sea ice cover or are largely driven by internal, natural variability of the atmosphere. Mori et al (2014) have suggested that as a result of sea ice reduction in the eastern Arctic, there is a higher frequency of Eurasian blocking events, and consequently the probability of severe winters has more than doubled in central Eurasia. Features such as cold winter conditions over the northern hemisphere mid-latitudes greatly affect a significant part of the population of Eurasia, and hence being able to predict such events is of great benefit for such communities.

This thesis investigates the impact of reduced sea ice conditions in the eastern sector of the Arctic Ocean on wintertime mid-latitude atmospheric circulation using a

numerical modelling approach. Prospects of making the understanding of Arctic-mid latitude links more robust are encouraging because implementing realistic sea ice initial conditions may provide additional predictability in climate forecasting (Jung et al., 2014), and in fact some studies have stressed the importance of realistic sea ice conditions for seasonal forecasts (Koenigk et al. 2016, Scaife et al., 2016).
In the remainder of this chapter, an overview will be given regarding observed changes in the Arctic cryosphere, followed by the evidence that exists for the impact of sea ice loss in the (eastern) Arctic on the mid-latitude winter climate, based on observational as well as modeling evidence. At the end of this chapter, the scope and objectives of the thesis will be presented.

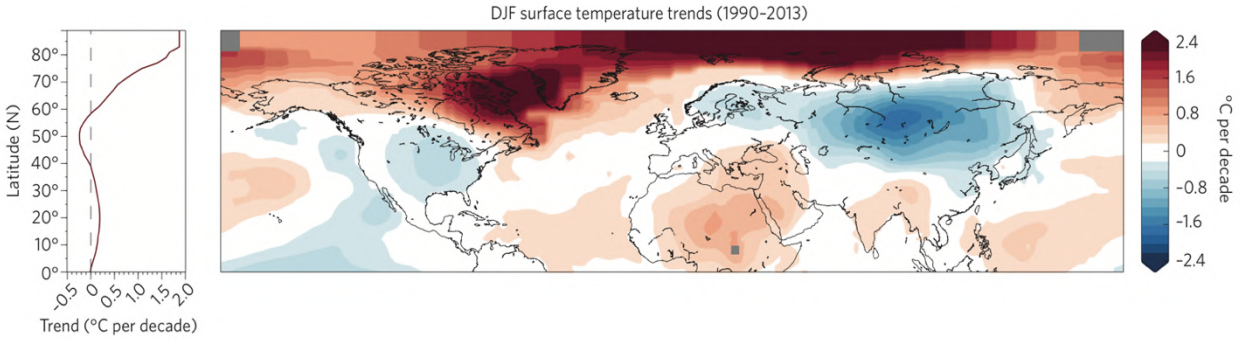

Fig. 1.1 Winter temperature trends from 1990-2013. Linear trend (°C per 10 years) in December-January-February (DJF) mean surface air temperatures from 1990 to 2013. Shading interval every 0.2°C per 10 years. *Adapted from Cohen et al., 2014.*

1.2 Arctic sea ice trends and the impact on the surface energy budget

The presence of Artic sea ice strongly modulates near-surface conditions at high latitudes, and potentially regional as well as global climate. Over much of the Arctic Ocean, low-level atmospheric temperatures and upper level ocean temperatures are as low as to allow sea water to be present in its solid state, sea ice. A sea ice cover present on the ocean changes surface albedo and acts as barrier for heat and momentum fluxes between ocean and atmosphere. Since the advent of satellite passive

microwave observing systems in 1979, it has been possible to monitor the entire extent of sea ice over the Arctic with a temporal resolution of less than a day.

Arctic sea ice reaches its maximum seasonal extent in February and March while the minimum occurs in September. In the Arctic, sea ice has overall declined and this decline is a function of season, region and age (thickness) of the ice. Averaged over the Arctic and on an annual mean basis, sea ice has been declining at a rate of 3.8% +/- 0.3% per decade. However, there exist large regional variations in these trends, as well as depending on the season in consideration. While during summer (JJA), the largest decline in sea ice cover occurs in the Laptev Sea and the East Siberian Sea, sea ice loss in autumn (SON) and winter (DJF) is dominated by the Chukchi and northern Barents Seas, respectively (Comiso, 2012). Between 1979 and 2012, the perennial sea ice extent (summer minimum) has declined by 11.5 +/- 2.1% per decade while the multi-year ice (that has survived two or more summers) decreased at a rate of 13.5 +/- 2.5% per decade (Comiso, 2008).
The increased energy absorption at the surface ocean that comes along with the newly ice-free areas has resulted in 4-5°C sea surface temperature anomalies over newly ice-free regions (Wood et al. 2013). The decrease in areal extent is accompanied by a decrease in mean winter (DJF) thickness since 1980 (Kwok and Rothrock 2009) and a 75-80% loss in volume (Overland et al. 2014). Related to these trends are also temporal shifts in the onset of the melting and re-freezing periods which result in a longer seasonal ice-free period (Vihma et al., 2014).
According to climate model projections, the loss in Arctic sea ice cover is going to continue. Although the accelerating trend in Arctic sea ice decline over the past two decades as revealed from satellite observations is a feature not captured by climate models participating in the IPCC Fifth Assessment Report, the central Arctic Ocean is predicted to be ice free in summer as early as the middle of this century (Stroeve et al., 2007).

Sea ice acts in modulating the Northern Hemispheric high-latitude surface energy budget by influencing the radiative, turbulent heat and momentum fluxes at the ocean-atmosphere interface (Serreze et al., 2007). High latitude surface turbulent heat fluxes are considerably larger in the boreal winter season (DJF) compared to the rest

of the year (here shown for summer (JJA); Fig. 1.3). This feature can be explained by contrasts in temperature and relative humidity between ocean and atmosphere which are maximal during winter. While the atmosphere near the surface may easily reach -30°C to -40°C during boreal winter, the ocean is still relatively warm due to the large ocean heat content compared to the atmosphere and mixing of this heat from below. In areas where there is sea ice, surface heat fluxes (in either direction) are heavily suppressed, even though depending heavily on ice thickness within the first 0.5m (Fig. 1.3). In fact, the ocean-atmosphere heat flux can vary by nearly two orders of magnitude between open water and an ocean covered with thick sea ice in wintertime conditions (Maykut, 1978).

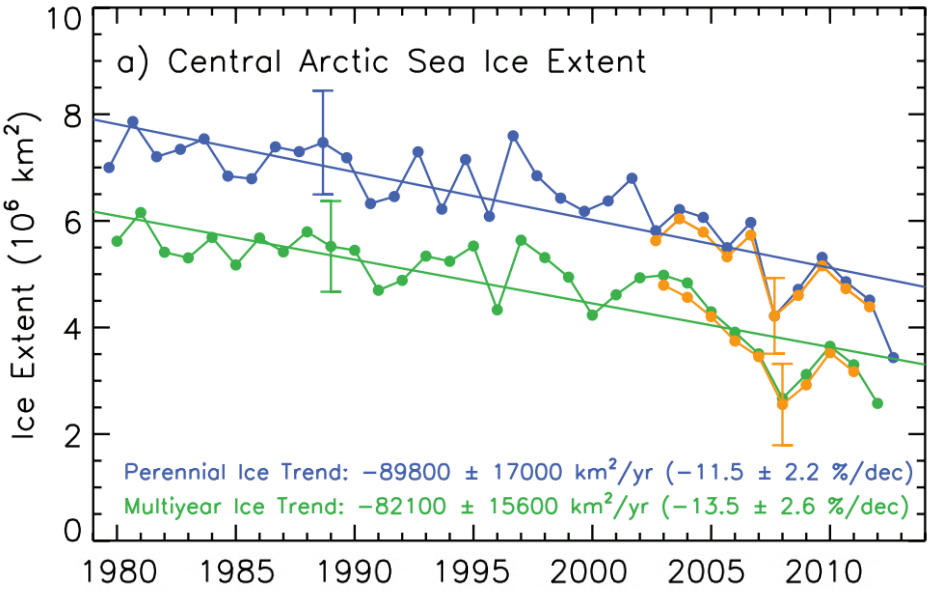

Fig. 1.2 Annual perennial (blue) and multi-year (green) sea ice extent (10^6 km^2) in the Central Arctic from 1979 to 2012 as derived from satellite passive microwave data. Perennial ice values are derived from summer minimum ice extent, while the multi-year ice values are averages of those from December, January and February (Adopted from Comiso, 2012).

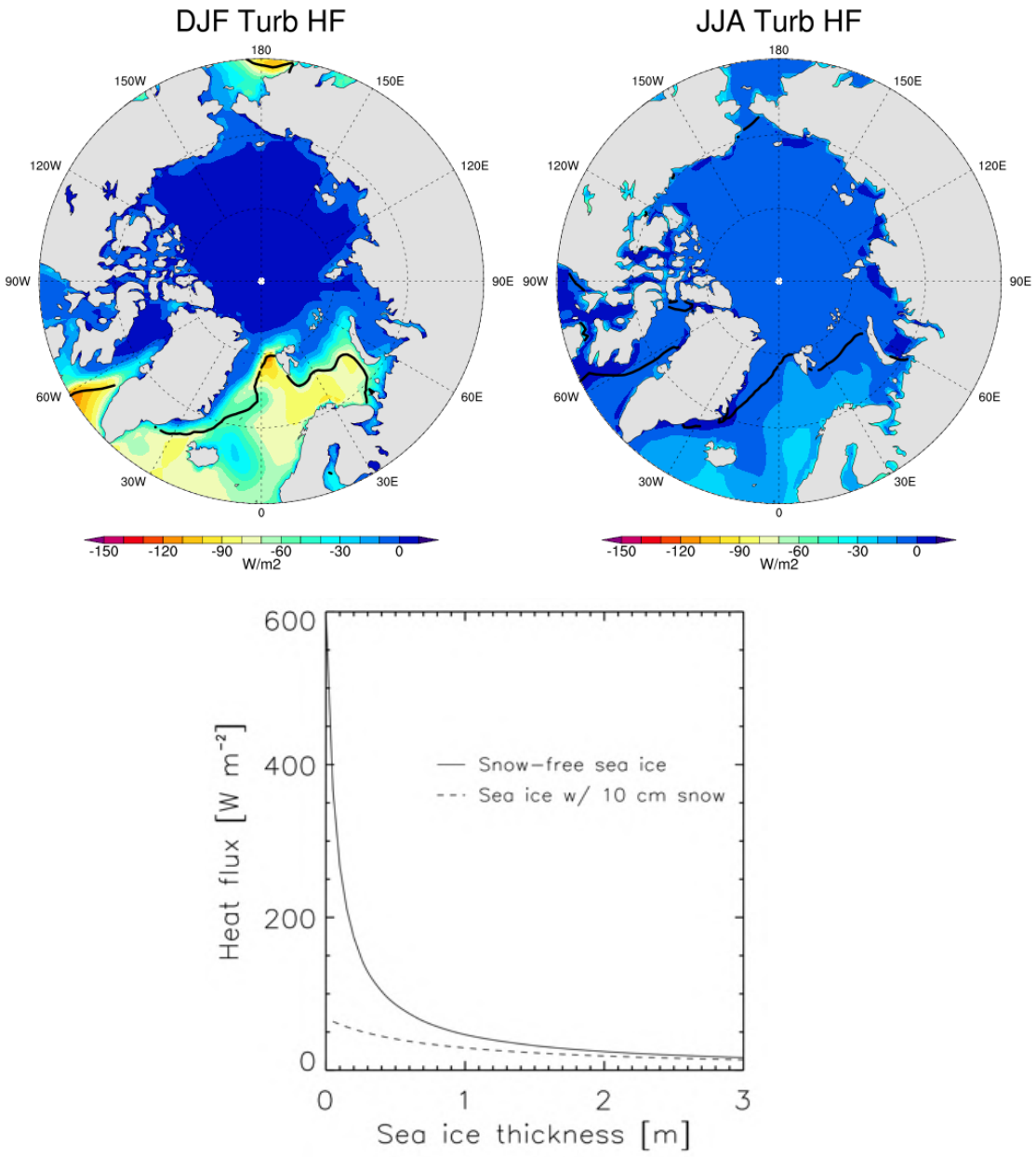

Fig. 1.3 a) and b) Turbulent surface heat fluxes (latent heat + sensible heat; THF) over the period 1979-2017 over the boreal winter season (DJF, a), and over the boreal summer season (JJA, ***b***), as obtained from re-analysis data (ERA-Interim). The black contour line indicates the climatological sea ice edge. **c)** Dependence of ocean-atmosphere heat fluxes (incoming longwave + emitted longwave + sensible + latent + conductive) on sea ice thickness for snow-free and snow-covered sea ice during typical winter time conditions. The data is obtained through a combination of freeboard data of ice thickness and a snow depth model (Kurtz et al., 2011).

1.3 The special case of the Barents Sea

The Barents and Kara Seas have increasingly become a focus in the recent years in the context of Arctic-mid-latitude linkages. The reasons for this emergence are briefly worth investigating. The Barents and Kara Seas (BKS) are marginal shelf seas situated in the eastern Arctic basin (Fig. 1.4), bordering the northern coasts of Norway and Russia and Siberia (Kara Sea). Due to its location the Barents Sea is the main pathway through which warm Atlantic waters enter the Arctic Ocean. The sea ice retreat in this area has been faster than anywhere else in the Arctic Ocean during the recent decades (>12% per decade; Parkinson and Cavalieri, 2008), and variations in BKS sea ice cover have been ascribed to a number processes: large-scale atmospheric circulation anomalies (Maslanik et al., 2007), increase in ocean heat transport (Årthun et al. 2012, cyclone activity (Sorteberg and Kvingedal, 2006), and even a remote impact from Gulf Stream SST's (Sato et al., 2014).

The BKS are the region of the Arctic Ocean which exhibit both a large trend and variability in sea ice and related surface turbulent heat fluxes during the boreal winter months (DJF; Fig. 1.5). The maximum in BKS SIC variability during autumn has been explained previously by a westward shift of maximum SIC anomalies from the Chukchi and East Siberian Seas in late summer (August, September) to the BKS sector in autumn (October and November; Yang et al. 2016). Some studies (Deser et al., 2010, Seierstad and Bader, 2009) have noted that the seasonal cycle of the climate response to sea ice loss anomalies follows the surface heat fluxes instead of the sea ice itself, and in this regard it is interesting to note that SHF (surface heat fluxes) peak in November in the BKS both in terms of linear trend and standard deviation over the period 1979 to 2013 (Yang et al., 2016). This circumstance leaves a potential impact of November sea ice anomalies in the BKS on local and regional climate during winter, and it is consistent with findings that identify November sea ice variability in the BKS as having the largest impact on the NAO (Koenigk et al., 2015).

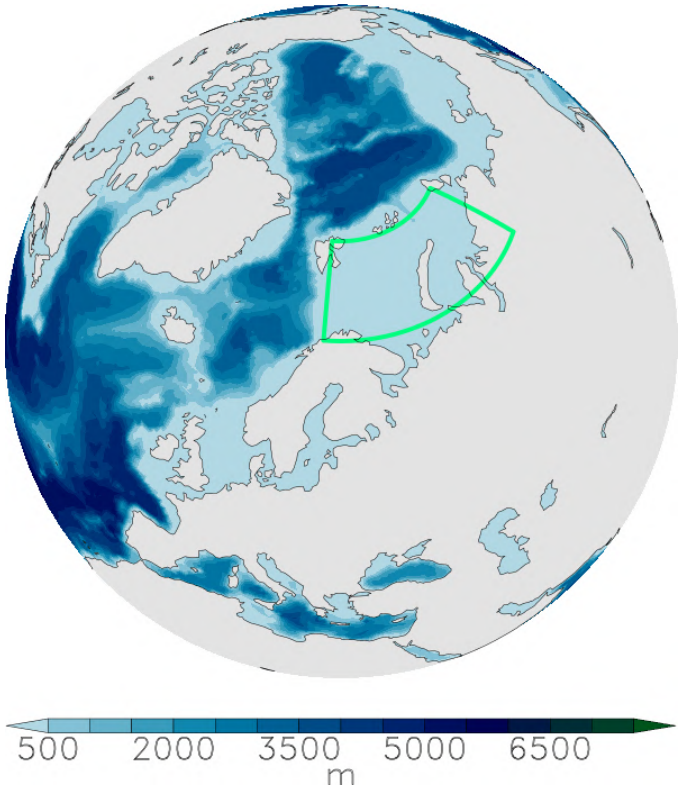

Fig. 1.4 Bathymetric map illustrating the geographical position of the Barents-Kara Seas (green rectangle) and the fact that they are shelf seas of the Arctic Ocean, as indicated by the shallow bathymetry (<500m).

1. 4 Evidence for the impact of Arctic sea ice loss on NH atmospheric circulation

1. 4. 1 Observational evidence

Evidence for sea ice impact on weather and climate on an observational basis stems mostly from reanalysis studies, whereas the immediate, local effects, are partly based on in-situ observations. Within a climatic context, Serreze (2009) and Screen and Simmonds (2010) have found that the recent anomalously large open water areas during September have resulted in a strong transfer of heat from the ocean mixed layer to the atmosphere, causing a large increase in surface air temperatures. Furthermore, a moistening of the boundary layer and decreases the near-surface static stability have been reported

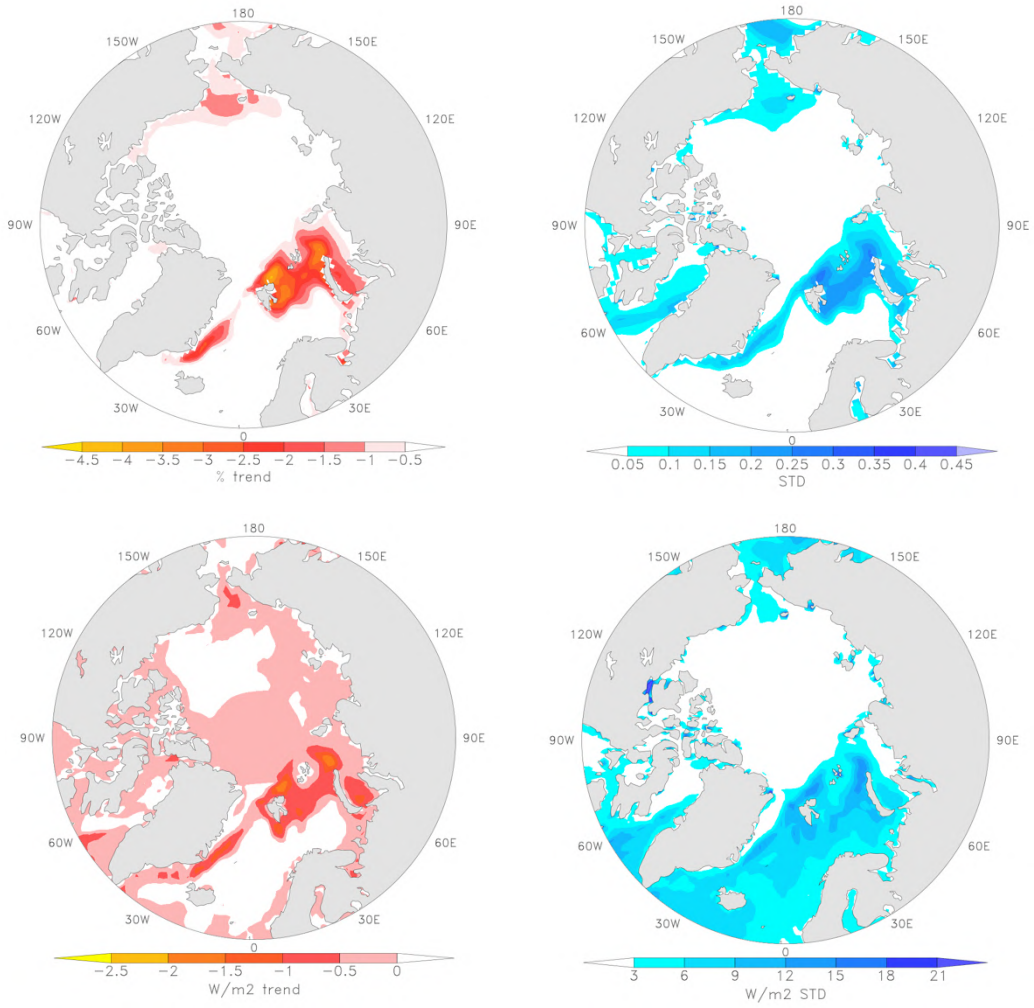

Fig. 1.5 Trend and standard deviation during winter (DJF) in the period 2000-2017, in sea ice cover (upper panel), and in turbulent surface heat fluxes (lower panel). Data are taken from the ERA-Interim re-analysis data set.

(Francis et al., 2009), a feature which was shown to make the atmosphere more liable to baroclinic instability and convection activity (Jaiser et al., 2012).

On a larger scale, the locally-generated surface warming as a consequence of sea ice loss has been found to weaken the meridional temperature gradient as well as increase the 1000-500hPa thickness in years of reduced sea ice cover (Overland and Wang, 2010). Nakamura et al., (2015), based also on a reanalysis study, have found a positive correlation between sea ice loss and the negative phase of the Arctic Oscillation (or

North Atlantic Oscillation), which is characterized by weaker and more equatorward mid-latitude westerly winds. An analysis based on geopotential height fields proposes an explanation of the observed persistence of weather extremes due to larger wave amplitudes and the associated slower eastward progression of upper-level Rossby waves Francis and Vavrus (2012). However, such views have been challenged based on the metrics chosen to define wave amplitude. In studies that apply a composite approach to study the impact of Arctic sea ice anomalies, it matters whether detrended or undetrended Arctic sea ice concentration are used for analysis. Undetrended SIC anomalies in autumn and winter result in changes primarily in the Pacific sector, such as changes in planetary wave propagation (Jaiser et al., 2012), while when using detrended SIC anomalies on the contrary, this caused a delayed atmospheric response largely in the Atlantic sector, resembling mostly an AO/NAO pattern there (e.g. Garcia-Serrano, 2015, Peings and Magnusdottir et al., 2014).

However, the shortness of the observational record and large atmospheric internal variability make the use of observational data challenging in inferring Arctic – mid-latitude linkages. In fact, the response inferred from statistical relationships using observational data sets may be opposite to the true response due to confounding factors (Smith et al., 2017). A correlation between SIC and atmospheric fields does not necessarily imply a physical relationship, and therefore it does not imply causality.

1. 4. 2 Evidence from AGCM and climate model studies

Given the constraints that observational data sets give us, the impact of sea ice loss on winter atmospheric circulation has been addressed using a hierarchy of numerical models. Sensitivity studies offer the possibility to isolate processes underlying the relationships that are found in observational studies. In studies that have adopted atmospheric general circulation models (AGCM's), a change in sea ice cover together with sea surface temperatures (SST's) is prescribed to the atmospheric model as a lower boundary condition. In fully-coupled models, a variety of approaches have been adopted in order to artificially manipulate the sea ice concentration, either in the sea ice or ocean model component (see below section 2.2.1 for different methods).

Atmospheric circulation anomalies have been studied in response to projected sea ice anomalies (Singarayer et al., 2006, Deser et al., 2010, Seierstadt and Bader et al., 2009, Peings and Magnusdottir, 2013), to prominent years that have shown a pronounced sea ice minimum (like 2007; e.g. Orsolini et al. 2012, Kumar et al. 2010, Porter et al., 2012), or over a longer period in the recent past (Screen et al., 2012). With respect to European winter climate, these studies have imposed sea ice anomalies in the Labrador, Greenland, and Barents-Kara Seas (BKS). In lines with what some of the observational studies suggest, a majority of the model studies indicate a circulation response that projects onto the leading mode of variability of northern hemisphere circulation, which for the Euro-Atlantic sector is the North Atlantic Oscillation (NAO). However, there has no consensus been reached regarding the sign of the NAO response. A number of studies point to a negative NAO-like circulation anomalies in mid- or late winter (Honda et al., 2009, Seierstadt and Bader, 2009, Alexander et al., 2003, Peings and Magnusdottir, 2013, Kim et al, 2014, Yang et al., 2016, Ruggieri et al., 2017), which is associated with colder and dryer winter conditions over northern Europe and eastern Asia due to a more southward displaced Atlantic jet and associated storm tracks. The 'warm Arctic – cold continents' pattern which is consistent with this negative NAO-like circulation pattern, has been increasingly observed during the last decades (Cohen et al., 2012). The negative AO/NAO response to reduced sea ice conditions has also been reported in observational studies (Honda et al. 2009, Wu and Zhang 2010). In contrast, other studies find a positive NAO-like response (Singarayer et al., 2006, Orsolini et al., 2012, Cassano et al., 2014), or an NAO response that is hardly (Screen et al., 2013, Petrie et al., 2015) detectable due to the large internal variability of the mid-latitude atmosphere. In studies where the dynamical cooling response over northern Europe/Eurasia (corresponding to a negative NAO event) is missing, a thermodynamical effect (the advection of warmed air masses) has been put forward to partly or fully offset the cooling signal (e.g. Screen, 2017). Some studies have reported changes in other aspects of the winter time circulation response that stand in relation to the negative phase of the NAO found late winter, such as a reduction in extratropical storminess (Seierstad and Bader, 2009).

1. 4. 3 Eastern Arctic sea ice variability and the WACS pattern

Section 1.3 has outlined the importance of the BKS in terms sea ice and related surface heat flux variability and trend, and hence their potential impact on winter atmospheric circulation. In fact, it could be shown that the BKS dominates in impacting Euro-Atlantic winter climate compared to sea ice loss in the other regions of the Arctic Ocean (Pedersen et al., 2016, Koenigk et al., 2016, Zhang et al., 2018), and an increasing focus of recent years has been the co-variability between sea ice anomalies in the eastern Arctic (Greenland-Barents-Kara Seas) and lagged atmospheric circulation anomalies in the Euro-Atlantic sector (Garcia-Serrano et al., 2015, Kim et al., 2014, Nakamura et al. 2015). The impact of sea ice loss in the BKS on Eurasian winter climate has been studied using simplified models (Zhang et al., 2018), intermediate complexity atmospheric models (Ruggieri et al., 2017), AGCM's (Petoukhov and Semenov, 2012, Kim et al., 2014, Sun et al., 2015), as well as coupled climate models (Smith et al., 2017, Deser et al., 2015). A common finding in most of the model but also observational studies regarding the atmospheric circulation response to eastern Artic sea ice loss (Greenland-Barents-Kara Sea) is an anti-cyclonic circulation anomaly over northern Eurasia, typically, at a lag of one month, that is consistent with the WACC pattern described above. This anomalous anticyclonic pattern in response to eastern Arctic sea ice has been many times identified as "precursor" of a negative NAO-like pattern that has been described above, i.e. positive and negative geopotential height anomalies at polar and mid-latitudes, respectively, over the Euro-Atlantic sector.

Depending on the timing of the response relative to the timing of the forcing (sea ice loss), two main pathways have been suggested to explain this transition to a hemispheric-wide circulation pattern (Garcia-Serrano et al., 2016). If the detected NAO-like response occurs with a lag of about 2 months, a positive feedback from transient eddy activity is suggested as a mechanism which resides in the troposphere. On the other hand, if the response is found at a lag of 1 month, a stratospheric pathway is suggested in which anomalous upward wave activity causes changes in the polar vortex strength which descend back to the troposphere projecting on a NAO-like pattern at the surface. This indirect mechanism has been the focus of studies in recent years, and has been detected in observational data (Ruggieri et al., 2016, King et al.,

2015) as well as AGCM studies (Kim et al., 2014, Sun et al., 2015, Ruggieri et al., 2017). The origin of SIC anomaly-induced changes in the upward wave activity and hence polar vortex strength lie in the troposphere. In particular, the anticyclonic anomaly described above tends to form a dipole anomaly of low pressure over central eastern Eurasia, and it is consistent with a Rossby wave train propagation in response to Barents-Kara SIC anomalies (Honda et al., 2009). Sun et al. (2015), based on an AGCM study, have noted that there is a competing effect in sea ice loss in the BKS versus sea ice loss in the Pacific sector, where anomalous waves destructively interfere with the background climatological flow, and hence sea ice loss imposed in both sectors results in a comparatively small stratospheric circulation response. In the identification of these pathways, in particular the month November has turned out crucial. Summarizing the evidence outlined above, sea ice loss in the BKS is crucial for two reasons for winter atmospheric circulation over the Euro-Atlantic sector. One the one hand, sea ice related surface heat fluxes variability and trend have their maximum in this region considering the whole Arctic Ocean, and on the other hand, negative sea anomalies in the BKS trigger anomalous planetary waves that are in constructive interference with the climatological background flow and have shown to affect stratospheric circulation with a potential surface impact in late winter.

While the above described dynamical pathways seem plausible, not all studies invoke the decline in Arctic sea ice as necessary in causing the warm Arctic – cold Siberia pattern (WACS; Sorokina et al., 2016, Scaife and Knight, 2008, Barnes 2013). Cold winter conditions, as they have occurred for example during the winter of 2005/06, have been ascribed to Atlantic SST anomalies and sudden stratospheric warmings (SSW) (Scaife and Knight, 2008, Croci-Maspoli and Davies, 2009). Such studies do not explicitly preclude that changes in sea ice could act in causing the WACS pattern but suggest there are other factors that can result in this near-surface temperature pattern. Taking this idea this to the extreme, some studies could show an influence of the atmosphere on sea ice producing similar statistical relationships as those of sea ice driving the atmosphere (Sorokina et al., 2016). In their study, Sorokina et al. find the leading turbulent heat flux (THF) variability over the BKS primarily driven by atmospheric variability instead of sea ice variability, and they come to the conclusion

that the WACS pattern is not a direct atmospheric response to Barents sea ice reductions.

Furthermore, Caian et al. (2017) have demonstrated a feedback process by which variability in Arctic sea ice lead the NAO index by 1 year which feeds back on the propagation of sea ice anomalies. Other studies, such as Zhang et al., 2008 relate large-scale atmospheric circulation anomalies to the recent accelerated decline in BKS sea ice retreat. In particular, in their study Zhang et al. have found that a switch from the tri-polar AO/NAO structure to a dipolar structure provides an accelerating impetus for the recent rapid Arctic climate system changes.
Clearly, considering pathways in both directions (atmospheric variability influencing BKS sea ice variability and *vice versa*), it can be argued that Arctic sea ice acts as both driver and response to atmospheric variability, as is argued at the beginning of this chapter. Consequently, it is vital to be able to properly disentangle cause and effect. To this end, this thesis makes a contribution in identifying and quantifying pathways that sea ice anomalies have on the atmospheric circulation in the boreal winter season.

1. 5 Scope and objectives of the study

The previous chapter has outlined the significance of sea ice for the climate system, but also the controversy that exists regarding exact pathways that connect late autumn sea ice loss in the BKS to large-scale circulation anomalies during (late) winter. The use of observational data is ambiguous in terms of cause and effect while model results seem to be largely model- and therefore state-dependent.
It is the aim of this thesis to tackle some outstanding questions of such linkages by using an innovative model experimental set-up. In particular, using a state-of-the-art seasonal prediction system, idealized sensitivity experiments are performed in which the November BKS sea ice cover is being perturbed repeatedly for 23 years of the modern hindcast (1993-2015) period using realistic initial conditions. This approach overcomes some important limitations in previous studies, that is, the impact of sea ice

loss is studied here across a range different winter conditions as they have occurred realistically in the recent past, instead of being representative of winter conditions in specific years (e.g. Orsolini et al. 2012, Kumar et al. 2010), or a future climate (Deser et al., 2010, Singarayer et al., 2006). In this way, the response that is assessed takes into account interannual variability that is related to dominant large-scale teleconnection patterns such as ENSO and the NAO. Furthermore, a noval way for keeping large parts of the BKS ice-free during late autumn (November) is presented, a month of the year that has turned out critical regarding the remote impact of BKS sea ice loss on winter Euro-Atlantic atmospheric circulation. This approach means a perturbation to the ocean model's surface heat. It is expected that using a fully-coupled modeling framework will give more a more realistic insight into sea ice-related climate impact due to the full ocean-atmosphere coupling as compared to using an atmospheric circulation model, however, noting also that increasing model complexity has its drawbacks (Screen et al., 2018). The model's predictive skill in terms of Arctic sea ice cover and some main characteristics of the northern hemisphere atmospheric circulation during winter will be assessed. A composite analysis approach will be adopted in which light sea ice years are contrasted with heavy sea ice years in the CMCC-SPS3 will help to identify the model's ability in simulating suggested Arctic - mid-latitude linkages.

Details on the components of the seasonal prediction system CMCC-SPS3, and the way sea ice free conditions are implemented are given in chapter 2. Chapter 3 is dedicated to the outcomes of the composite approach and sensitivity experiment with reduced ice in the BKS. These results will be discussed in chapter 4. Chapter 5 summarizes and concludes this study with an outlook for future prospects.

2 Methods

2. 1 The CMCC-SPS3

2. 1. 1 Structure and model components

The impact of sea ice anomalies in the BKS on the climate of the following winter season is studied using the CMCC Seasonal Prediction System version 3 (CMCC-SPS3). It is a fully-coupled atmosphere-ocean-land-ice model that is used in operational mode by the Euro-Mediterranean Center for Climate Change (CMCC) to issue seasonal forecasts. CMCC-SPS3 is based on the CMCC Climate Model 2 (CMCC-CM2), which is a version of the Community Earth System Model (CESM) with a replacement of the ocean model component POP (Parallel Ocean Programming) by the Nucleus for European Modelling of the Ocean model (NEMO; Fogli and Iovino, 2014). The CMCC-SPS3 consists of atmosphere, ocean, land and sea ice and components that are connected through a coupling unit that controls the execution and time evolution of the system as well as communicating fluxes between the model components. Figure 2.1 gives an overview of these components. The CESM can be regarded as a state-of the-art model for simulating Earth's atmosphere, land, ocean and land and sea ice components in past, present and future climate states. In the following sections, a brief description of the single model components and the model bias is given, as well as the way in which the model ensembles are generated. This is followed by a description of how ice-free conditions are achieved in the NEMO 3.4 ocean model, and the data sets being used for the analysis.

The atmosphere

The atmospheric component of CMCC-SPS3 is represented by the Community Atmosphere Model version 5 (CAM5.3) which can be configured to use a spectral transform, a finite volume or a finite elements dynamical core. The atmosphere implemented in the CMCC-SPS3 runs in the spectral element configuration (a

formulation of the finite element method that uses high degree hybrid polynomials as basis functions), with a horizontal resolution of about, 46 vertical levels up to about 0.3hPa. This configuration allows for a proper representation of the stratospheric processes that are relevant for this study (such as vertical Rossby wave propagation and wave breaking) and stands in contrast to its precursor version CAM4 with 30 model levels and a top-of-the atmosphere at ca. 3hPa (Sanna et al., 2017). The horizontal resolution adopted here is 1° (about 110 km) and the integration time-step is 30 minutes.

The ocean

The ocean is represented by the eddy-permitting version 3.4 of the NEMO ocean model (NEMO3.4) with a horizontal resolution of ¼°(about 25 km), 50 levels (31 in the first 500 m) and an integration time-step of 18 minutes. The prognostic variables are the three velocity components, the sea surface height, the potential temperature and the practical salinity. The model uses a filtered, linear, free-surface formulation, where lateral water, tracers and momentum fluxes are calculated using fixed-reference ocean surface height. The time integration scheme used is a Robert–Asselin filtered leapfrog for non-diffusive processes and a forward (backward) scheme for horizontal (vertical) diffusive processes (Sanna et al., 2017). The model uses an isotropic curvilinear orthogonal grid with an Arakawa C–type three-dimensional arrangement of variables in the horizontal direction. Here, a tri-polar ORCA-like grid is used which has two poles in the Northern Hemisphere (in Siberia and in Canada) and one in the Southern Hemisphere that is co-located with the geographic South Pole.

Sea ice

The sea ice component is version 4 of the Community Ice Code (CICE4) which is the latest version of the Los Alamos Sea Ice Model. As the NEMO ocean model, the CICE4 model is integrated on the curvilinear ORCA grid, however with an integration time step of 30 minutes. The model includes the thermodynamics of Bitz and Lipscomb (1999), the elastic–viscous–plastic dynamics of Hunke and Dukowicz (2002),

and a sub-grid scale representation of ice thickness distribution following Thorndike et al. (1975). Two of the notable improvements compared to an earlier version of the model is the capability to simulate explicitly melt ponds and the deposition and cycling of aerosols (dust and black carbon) within the ice pack. These new capabilities influence both the mean climate state and simulated climate feedbacks at high latitudes (Holland et al., 2012).

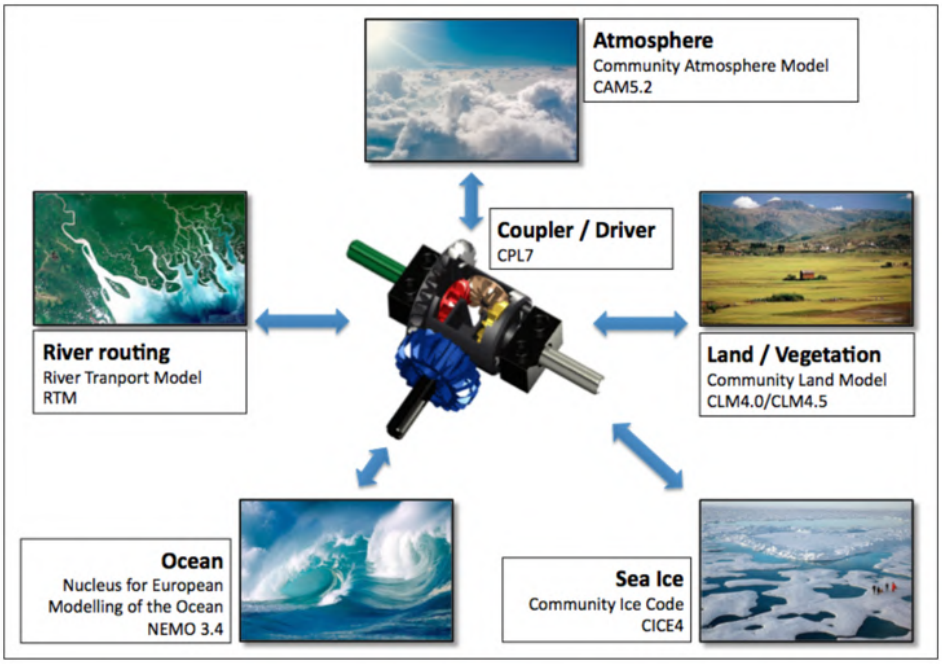

Fig. 2.1 Schematic of the CMCC Seasonal Prediction System version 3 (CMCC-SPS3) consisting of atmosphere (CAM5.2), land (CLM4.5), ocean (NEMO3.4, ice (CICE4), river routing (RTM) and coupler (CPL7) units. *Adopted from Fogli and Iovino, 2014.*

The Land Surface

The land surface component is the Community Land Model (CLM4.5) (Oleson et al., 2013); which captures the physical, chemical and biological processes by which terrestrial ecosystems affect and are affected by climate, across a variety of spatial and

temporal scales. Terrestrial ecosystems, through their cycling of energy, water, chemical elements, and trace gases, are important determinants of climate (Fogli and Iovino, 2014). The land model is integrated on the same grid as the atmosphere (1°x1°). Using an annual time series of the spatial distribution of plant functional types (PFTs) and wood harvest, CLM4.5 diagnoses the change in area for each PFT at every model time step by performing mass and energy balance that cause variations of PFT area during the six-month integration (Sanna et al., 2017). New features relative to previous versions of CLM include a prognostic carbon–nitrogen (CN) model an urban canyon model (Oleson et al. 2008) and a transient land cover and land use change capability, including wood harvest (Lawrence et al. 2012a).

2.1.2 Initialization strategy and ensemble generation

The atmospheric component is initialized, for all historical re-forecasts, with data from the ERA-Interim reanalysis product (Berrisford et al., 2009). The initial conditions for the ocean and the sea-ice components are provided by the monthly reanalysis of the eddy-permitting C-GLORS ocean data assimilation system (Storto et al., 2011). For the re-forecast period used in this study, the ocean and sea ice initial conditions stem from re-analysis data of the period 1993-2016. The initial conditions for the sea-ice component are produced at the same time as the ocean reanalysis. The initialization of the land component is achieved through a Land Data Assimilation System (LDAS, Koster et al., 2009). The technique consists of forcing a land-surface model (CLM4.5, the Common Land Model version 4, i.e. the land component of SPS3, uncoupled from an atmospheric model) with observed, near-surface meteorological fields.

In order to account for the uncertainty associated with the initial conditions when performing seasonal forecasts, 40 perturbations of the initial state are produced for the standard re-forecasts. Perturbations are generated by combining the initial states of the three main model components: 10 for the atmosphere (of the tropospheric layers), 4 for the ocean and 3 for the land surface. This results in 120 possible combinations (10 x 4 x 3); from there, 40 unique combinations are randomly chosen that compose the CMCC-SPS3 initial conditions set.

The following lists the procedure in which initial conditions are generated for each model component.

- **Atmosphere.** The atmospheric initial conditions are provided by the ERA-Interim operational analysis at 00z UTC on day 1 of the start month. Further nine alternative initial conditions are generated with a time-lagging technique going back in time from the original start date (initial states taken every 24 hours).

- **Ocean.** Both the assimilated observations and the atmospheric forcing (winds, short- and long-wave radiation, 2-meter temperature and specific humidity, precipitation) of the control ocean data-assimilation model are perturbed. The observations are perturbed by adding a random error proportional to the mean observational error. The atmospheric forcing perturbation is constructed by computing, for each month and each variable, the daily differences between the atmospheric forcing datasets (NCEP and operational ECMWF or ERA-Interim), and randomly adding one of these field differences to each daily forcing.

- **Land-surface.** Land surface is perturbed by modifying the atmospheric boundary conditions (2-meter temperature, sea level pressure, 2-meter specific humidity, 10-meter winds, precipitation and surface solar radiation) in the land component forced simulation. The required variables are derived using three datasets: ERA-Interim, NCEP and a linear interpolation of the two. With this forcing imposed every three or six hours, CLM4.5 produces three comparable restarts that are used as initial conditions.

It could be argued that the perturbation applied to the atmospheric component of CMCC-SPS3 are comparatively small, given that initial states are separated by only 24 hours. It should be noted that other seasonal forecasting systems use only round-off

perturbations, which are much smaller than these arising from a 24-hour lag. Perturbations are supposed to address the uncertainty in the initial conditions and therefore should be comparable in amplitude, or smaller, than the observational uncertainties. Current state-of-the-art ensemble generation techniques in seasonal forecasting are not as advanced / elaborate as the ones developed for weather prediction.

2.1.3 Model Biases

This section gives a brief overview of model biases that are known for CMCC-SPS3, and that affect its mean climate state and climate sensitivity. The atmospheric response to sea ice loss has shown to be model- and therefore state-dependent (Smith et al., 2017), hence identifying model biases can be crucial in order to assess the model's response to sea ice loss. Here, biases are evaluated for near-surface temperature, T_{850} and precipitation, and will be extended upon in section 3.1. They are here reported by lead season relative to the start date, i.e. NDJ (lead season 0), DJF (lead season 1) and JFM (lead season 2). The model mean winter climate is compared to reanalysis data set (ERA-Interim) over the same time period (1993 – 2016).

For the November start date, there is a pronounced negative 2m-temperature bias over northern hemisphere northern continental areas of North America, Greenland and Eurasia of about -2°C to -4 C° while the opposite is true for the Arctic basin with a positive temperature bias of about 2°C to 4°C (Fig. 2.2, left). There are some positive biases of circa 1.5°C to 2°C over the temperate continental areas of Eurasia. The bias is generally much reduced over other oceanic regions and in the southern hemisphere where it is nearly zero. A different pattern can be observed for 850hPa temperature (Fig. 2.2, right) in which a slight negative bias can be seen in the high latitudes and in the tropical Pacific and the South American coastal Pacific (the main El Niño region). High mountain areas (e.g. Greenland, Himalaya, Andes and the Rockies) should be disregarded since the 850hPa isobaric surface is below ground and there temperature is extrapolated from above and therefore affected by large errors (Sanna et al., 2017).

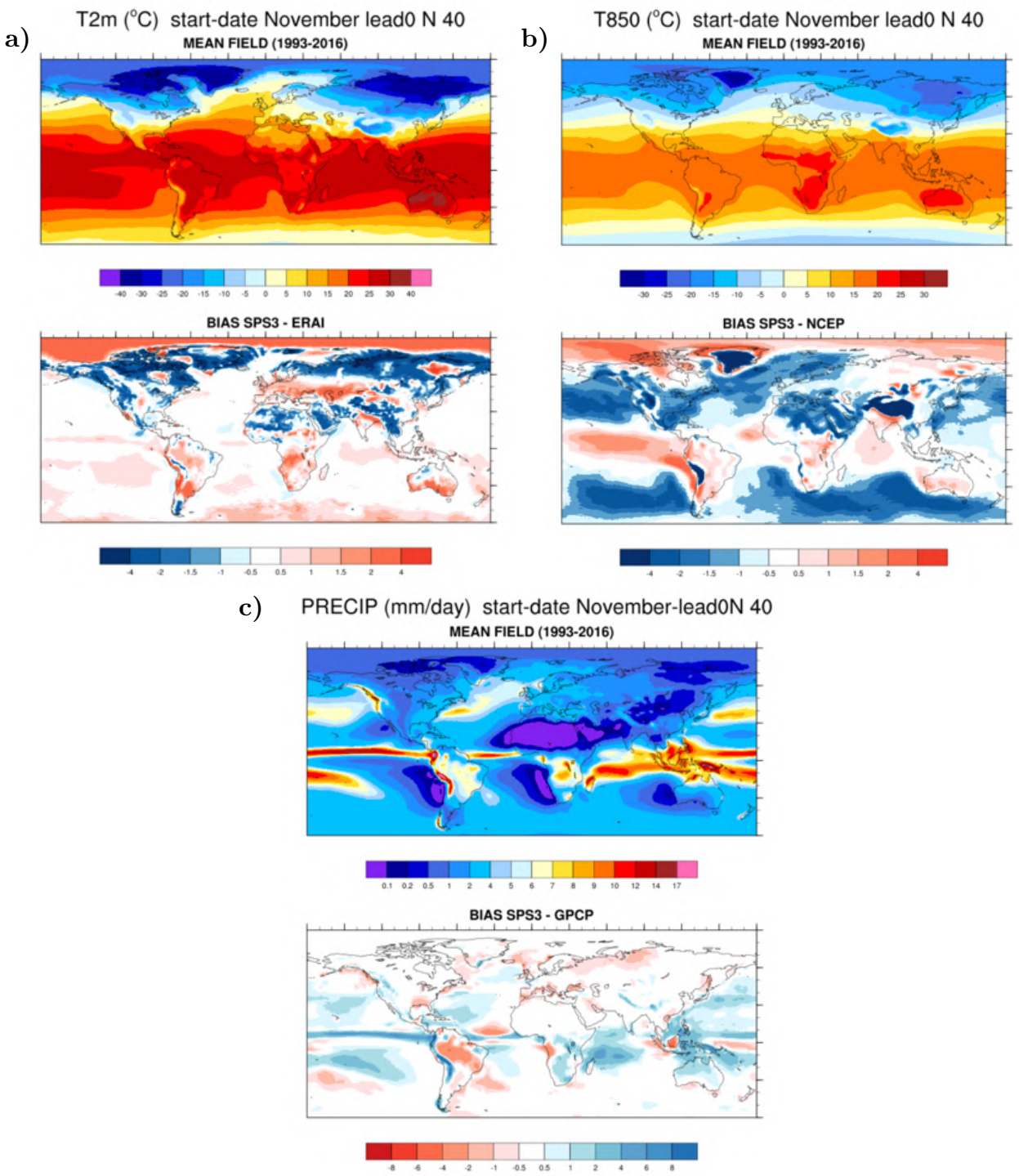

Fig. 2.2 Model three-monthly mean field and biases relative to ERA-Interim and NCEP re-analyses (lower panels) for November start date of **a)** 2m-temeprature **b)** temperature at 850hPa and **c)** precipitation. Lead time 0 refers to the model mean of the first 3 forecast months (i.e. NDJ). The mean refers to the ensemble mean of 40 members for each year in the hindcast period 1993-2016. *Adopted from Sanna et al., 2017*

Regarding the precipitation bias, the typical double Intertropical Convergence Zone in the tropical Pacific basin is apparent for CMCC-SPS3, as it is for many state-of-the-art climate models. Generally, the precipitation bias is in the range of 2-4 mm $day^{-1}$and is less pronounced over Northern Hemisphere mid-latitudes and polar regions.

2. 2 Data set and experimental set-up

2.2.1 Data for composite analysis

As outlined at the end of Chapter 1, a composite analysis approach is adopted that serves to assess the model's ability to capture the atmospheric response to sea ice reduction. The data set used for the composite analysis is taken from output of hindcast simulations using the CMCC-SPS3 in the time window 1993-2015. The forecast simulations each last 6 months, with a start at November 1st (hence 1 November – 30 April). The mean of 40 ensemble members are taken into account for the analyzed fields (ice cover, surface heat fluxes, 2m-temperature, mean sea level pressure, geopotential height at 500hPa, zonal winds at 250hPa). The ERA-Interim (European Centre for Medium-Range Weather (ECMWF) Re-Analysis) product is used to assess the atmospheric response to sea ice loss in observations. The fields of interest have been extracted on a six-hourly basis on a 1-degree, regular, global latitude/longitude grid (Dee et al., 2011).

The years that define low and high sea ice cover in the BKS sector are defined based on the November mean sea ice concentration in the BKS sector over the area (15°-90°E, 75°-80°N). Years of low sea ice and high sea ice concentration are defined, correspondingly, as those falling below the 10th percentile and those remaining above the 90th percentile of the detrended mean sea ice concentration anomalies (Fig. 2.3). Thus, the low sea ice years are: 1995, 2012, 2016 (entitled 'LOW') and high sea ice years are: 1998, 2006, 2014 (entitled 'HIGH'). Low and high sea ice years in the observational record are defined according to the same criterion and result in 1996, 2000, 2009, 2012 as low sea ice years and 1998, 2002 and 2014 as high sea ice years. The National Snow and Ice Data Center (NSIDC) sea ice data has been used in order to define the composite based on the fact that it is intrinsically observed sea ice cover by means of satellite microwave radiometry. The ERA-Interim data set that is used for

the atmospheric fields shows the same maxima and minima in terms of sea ice concentration (not shown). For both model and re-analysis data, the response is defined by the difference between LOW sea ice years and HIGH sea ice years (i.e. fields from LOW sea ice years are subtracted from fields from HIGH sea ice years).

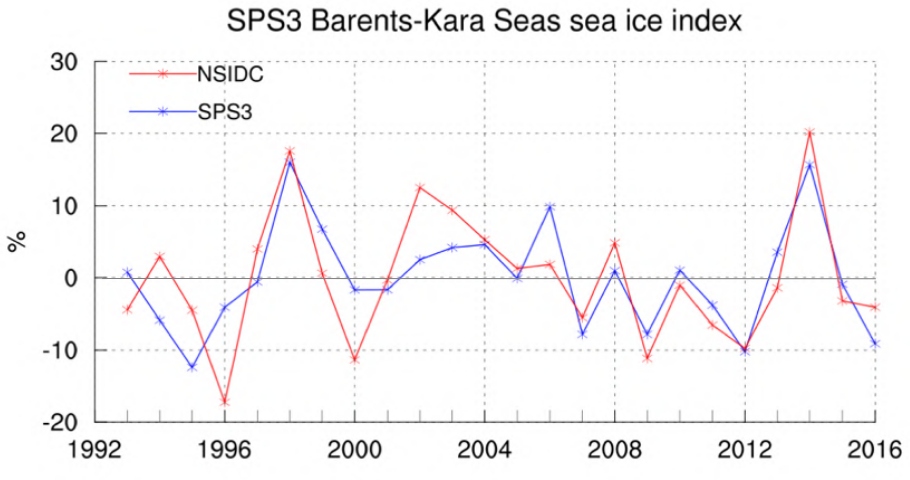

Fig. 2.3 Detrended November mean sea ice concentration, as simulated by the model (blue) and as observed by satellite imagery (NSIDC, red). The observed sea ice concentration time series is taken from the National Snow and Ice Data Center (NSIDC).

Detrended fields are considered for the analysis and the seasonal cycle is removed as well. The background for this choice lies in the interest to study the atmospheric response to sea ice concentration extremes around the mean, leaving potential changes related to long-term trends due to the global warming signal aside, as has been followed previously (e.g. Garcia-Serrano et al., 2015).

2.2.2 Data set for the sensitivity experiments

For studying the atmospheric response to reduced ice conditions in the BKS for different years across the model's hindcast period, the seasonal forecast simulations with November start date (previous section) are repeated for 10 members in each year in the period 1993-2015, with the only difference that the ocean model's surface heat

budget is perturbed in the BKS during November as described in section 2.2.1 in order to achieve the desired effect of sea ice loss/reduction. This experiment is referred to as "ICE-FREE" while the control, unperturbed experiment is called "CTRL" in what follows. The control simulation for this experiment is identical to the simulations described above in "composite analysis", with the difference that only members for each year are considered that are identical to the ones in ICE-FREE (hence 10 for each year). The response to ice loss is defined by subtracting the fields in ICE-FREE from the fields in CTRL, similar to the approach of the composite analysis (subtracting LOW from HIGH, section 2.3.1). Table 1 summarizes the experimental set-up used in this study, with characteristics that are shared between the experiments and others which differ between them.

The statistical significance of the difference between the perturbed (ICE-FREE) and control (CTRL) simulation has been computed according to a test for differences of the mean for paired samples (Wilks, 1962). The following test statistic has been used:

$$z = \frac{\overline{\Delta} - \mu_{\Delta}}{(s_{\Delta}^2/n)^{\frac{1}{2}}}$$

where $\overline{\Delta}$ is the difference between the means of the two samples, μ_{Δ} is the corresponding population mean, here taken zero under the Null hypothesis, s_{Δ}^2 is the sample variance of the n differences between the two samples (n=23x10=230 for the data set here). The statistical significance has been evaluated at the 95% confidence interval.

Experiment / Characteristics	ICE-FREE	CTRL
Start date	November 1st	
Period simulated	1993-2016	
Integration length	6 months	
Ensemble size	10	10
Ocean component (horizontal resolution)	NEMO 3.4 (0.25°)	
Atmosphere component (horizontal resolution)	CAM 5.2 (1°)	
Ocean upper boundary restoring	dQ/dT = -5000 W/m^2	-

Table 1: Summary of experiments performed in this study with CMCC-SPS3.

2.3 Performing sensitivity experiments with CMCC-SPS3

2.3.1 Implementation of reduced sea ice conditions in NEMO 3.4

As outlined in section 1.3.4, a number of studies have shown a sensitivity of the atmospheric circulation in late winter to sea ice loss in the eastern Arctic (BKS), particular during November. For this purpose, an anomalous state with a considerable loss in sea ice fraction in the BKS is implemented in the ocean model component of CMCC-SPS3 (NEMO 3.4) during the month of November, the 1st month of the seasonal forecast integration.

In previous studies, different approaches have been adopted in order to achieve a loss in sea ice cover and/or a priori prevention of sea ice formation. These approaches range from a reduction in the albedo parameter (Blackport and Kushner, 2016), that increases the absorbed solar shortwave radiation, to experiments that allow sea water to cool below freezing point (Cvijanovic and Caldeira, 2015), and to altering the sea ice thickness as initial condition which causes enhanced summer melt (Petrie et

al., 2015). Even though in each of these approaches it is the ultimate goal to introduce a change in the sea ice component, the precise methodology differs which has consequences for the conservation of mass (water) and energy budgets. Any imposed anomalies can eventually propagate through the entire coupled system and alter air-sea interaction and/or oceanic circulation which can result in a disturbed model equilibrium. There are advantages and disadvantages for every different approach. The method followed here is a combination of flux adjustment and a nudging procedure. Following the method by Haney (1971), additional heat is supplied to the mixed layer of the ocean model component (NEMO 3.4) in the following way. SST's are restored through the introduction of a negative feedback term that is added to the non-solar heat flux:

$$Q_{ns} = Q_{ns}^{0} + \frac{dQ}{dT}\left(SST_{model} - SST_{target}\right) \quad (1)$$

where Q_{ns} is the corrected sum of the non-solar surface heat flux budget terms, Q_{ns}^{0} is the initial, uncorrected non-solar heat flux, dQ/dT is a retroaction coefficient ($W/m^2/K$), SST_{model} is the model's sea surface temperature at each consecutive time step and grid point, and SST_{target} is the targeted SST to which the model SST's are nudged to at each model time step. Nudging of SST's is applied in a conditional manner, so as to disturb the model equilibrium as little as possible, yet in a way to keep SST's above freezing. Nudging takes place only when SST's are equal or smaller than -1.5°C (approaching the freezing point of ca. -1.75°C for seawater with a salt content of ca. 35psu):

$$Q_{ns} = Q_{ns}^{0} + \begin{cases} \frac{dQ}{dT}\left(SST_{Model} - SST_{Target}\right), & if\ SST \leq -1.5 \\ 0 & otherwise \end{cases} \quad (2)$$

The proximity of the temperature threshold to the freezing temperature of seawater requires a large heat input in order to make the nudging efficient. Here, a retroaction term of dQ/dT=-5000 W/m²/K is chosen which is two orders of magnitude larger than the default value (-40 W/m²/K; Cassou et al., 2016), but is an approach that has been followed in previous studies. Luo et al. (2005) have chosen a retroaction term 60 times larger than default and Keenlyside et al. (2008) have chosen a retroaction term 15 times larger than default.

The above tendency equation is applied by means of a mask which weighs equation (1) in the range [0,1]. The mask is shown in Figure 2.4. The restoring to ice-free[1] conditions is applied in a core area that covers the northern part of the Barents Sea and the entire Kara Sea. This area resembles or in fact slightly exaggerates the area of the largest trend and variability in sea ice cover over the observational period (Fig.1.2), but it will be shown in section 3 that the effective sea ice removal averaged over all years represents very well the area of largest sea ice loss and variability in the BKS.

A buffering zone is implemented at the boundaries of the mask that reduces the weights gradually down to zero in order to avoid unreasonable horizontal gradients in SST's and heat fluxes at those boundaries. The southern part of the Barents Sea is excluded from the restoring and the mask because the climatological sea ice edge never migrates south of about 75°N during November in this region. Averaged over all years, the resulting sea ice cover in ICE-FREE mimics a typical minimum year (here shown for 2012) in terms of sea ice cover in the BKS (Fig. 2.5), despite a very weak fading of very low sea ice concentrations in the northern Kara Sea.

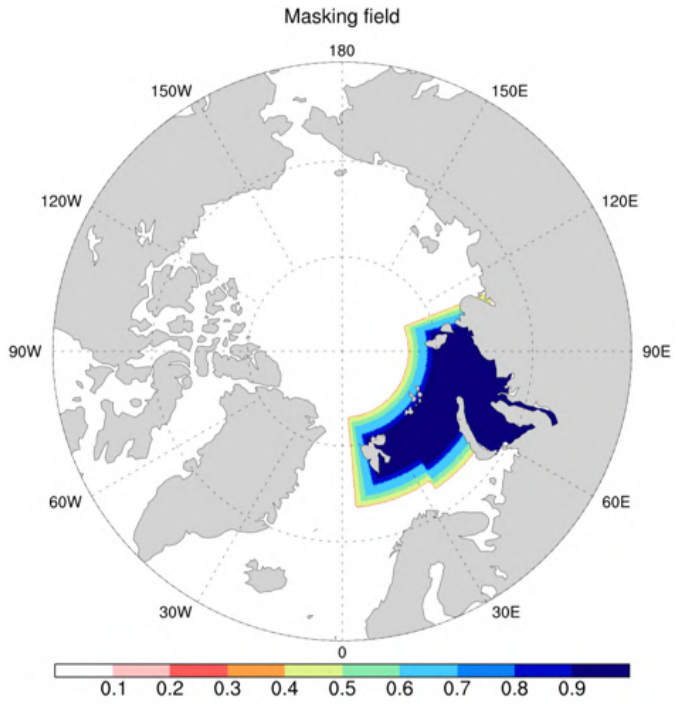

Fig. 2.4: Masking field applied to the tendency equation (Equation 1 above).

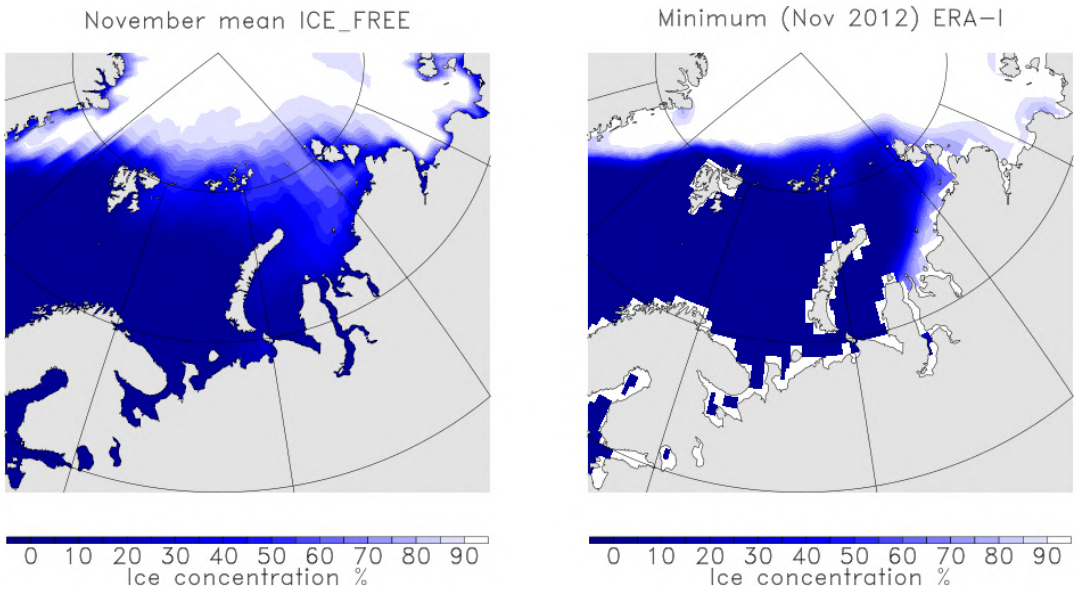

Fig. 2.5 November mean sea ice concentration in the BKS sector. *Left:* in the ICE_FREE experiment averaged over all years (1993-2015). *Right:* as observed from ERA-Interim during a typical minimum year (here shown for 2012).

3 Results

3. 1 Assessment of model performance: winter mean climate and inter-annual variability

This section explores some main characteristics of the model's mean winter climate in the Arctic and its variability over the period 1993-2015. The model's climatology for sea ice cover and surface heat fluxes as well the predictive skill for winter sea ice cover are presented, besides selected diagnostics for mid-latitude atmospheric fields.

3. 1. 1 Arctic sea ice concentration and surface heat fluxes

The Arctic sea ice extent as simulated by the model for November and winter (DJF mean) is in overall agreement with the observations regarding the position of the outer sea ice edge (Fig. 3.1, top). The simulated sea ice, however, shows reduced sea ice cover over large parts of the Arctic Ocean in both November and DJF mean compared to observations which results in a small negative bias over large parts of the Arctic Ocean (Fig. 3.1 upper right). The DJF mean reveals also a positive bias off the east coast of Greenland along the East Greenland current where the model overestimates the sea ice concentration. This relatively small bias arises from the respective sea ice edge being further off the coast in the model in respect to observations. During both November and in the DJF mean, the model seems to underestimate the sea ice interannual variability in the Barents Sea, near the Bering Strait (November) and in Hudson Bay (November) and in the Labrador Sea (DJF), while it overestimates it in Baffin Bay and to the east of Greenland throughout all the winter season.
Area-averaged properties over the BKS sector (Fig. 3.3) give us a better estimate of the model's performance in this area. The area-average of all fields is computed based on the core area of the masking field controlling the SST restoration for the sensitivity experiments (cf. Fig. 2.3; 15°E-90°E, 75°E-80°E). Corresponding to the deficit in the

simulated ice cover (Fig 3.1), the surface sensible and latent heat fluxes exceed the ones from re-analysis (ERA-Interim).

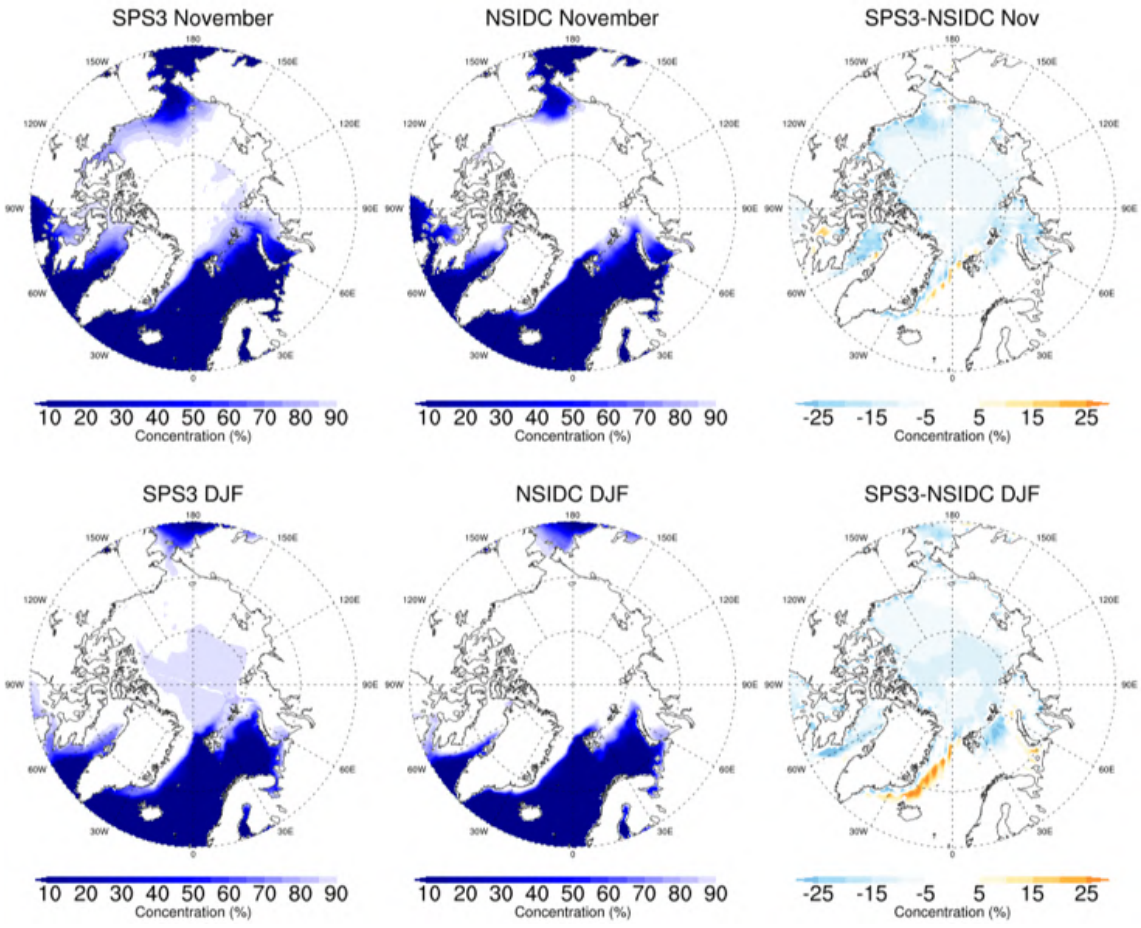

Fig. 3.1 Simulated (SPS3; left) and observed (NSIDC; middle) sea ice concentration during November (upper row) and the DJF mean (lower row), and their difference (right column).

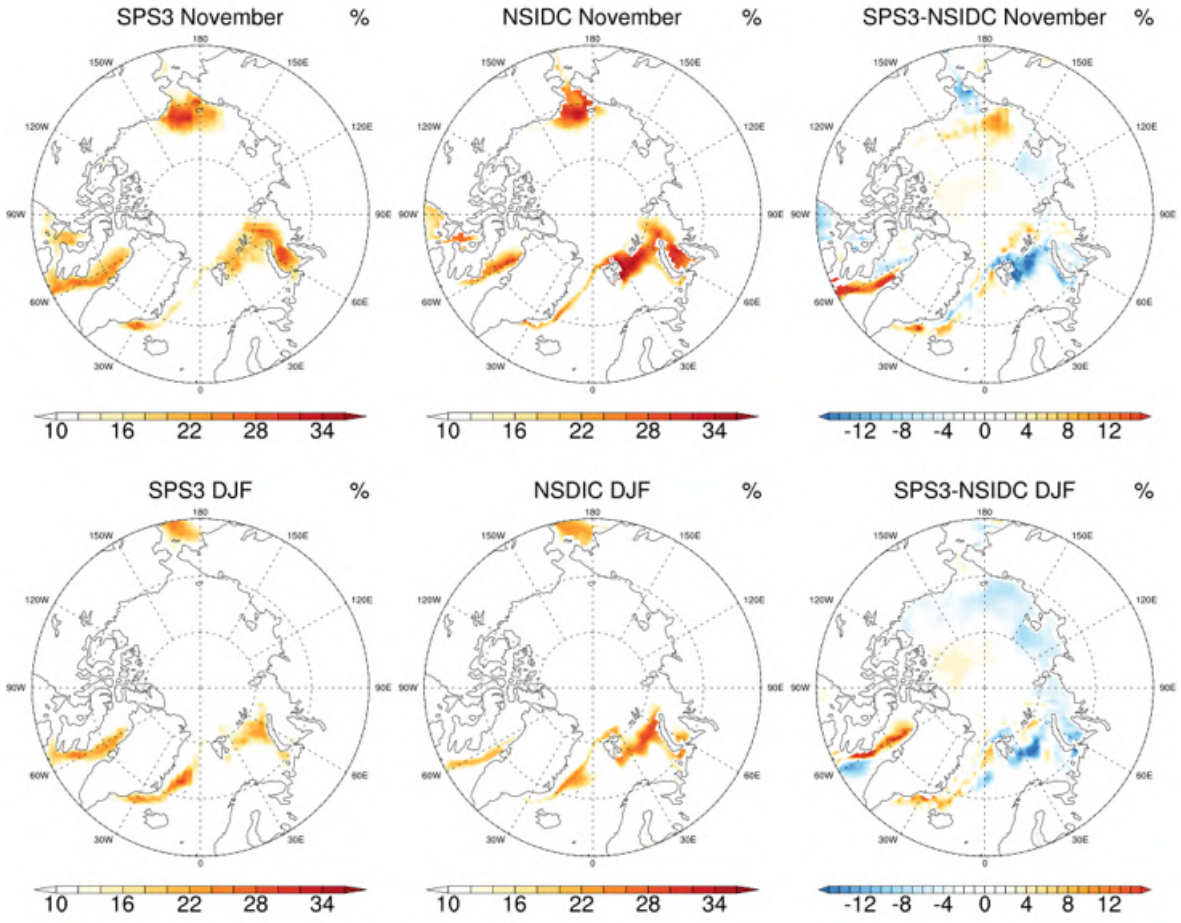

Fig. 3.2 Simulated (SPS3; left) and observed (NSIDC; middle) standard deviation of sea ice concentration during November (upper row) and the DJF mean (lower row), and their difference (right column).

Observations (cf. Fig. 1.2) revealed the largest trend in sea ice concentration in the BKS sector to occur in November, a feature that is shared with the simulated sea ice cover (Fig. 3.4 a, b). November is then followed by December, January and February (SPS3) and by February, December and January (NSIDC). Even though the trend is not considered for the analysis, this information contributes to the overall model assessment.

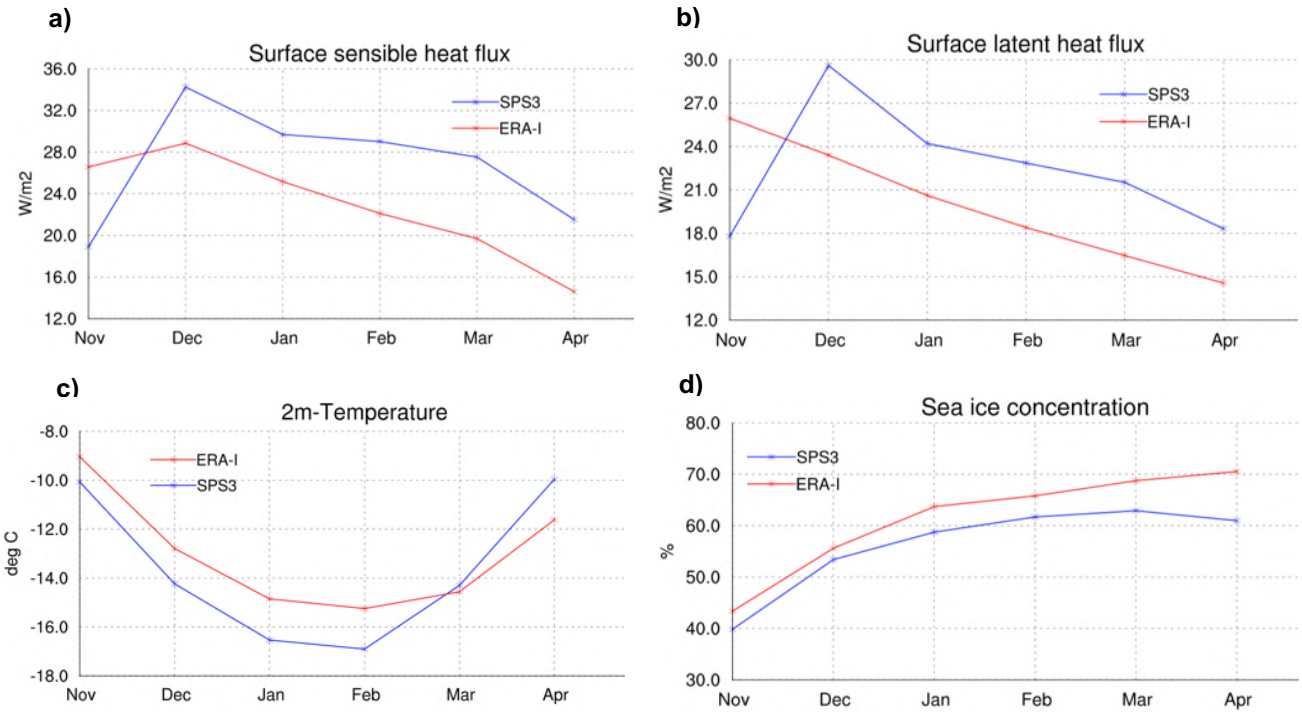

Fig. 3.3 Simulated (SPS3) and observed (ERA-Interim) winter climatology of (a) surface sensible heat flux (W/m^2), (b) surface latent heat flux (W/m^2), (c) 2-meter temperature (°C) and (d) sea ice cover (%) over the Barents-Kara Seas (15°E-90°E, 75°N-80°N) over the period 1993-2016.

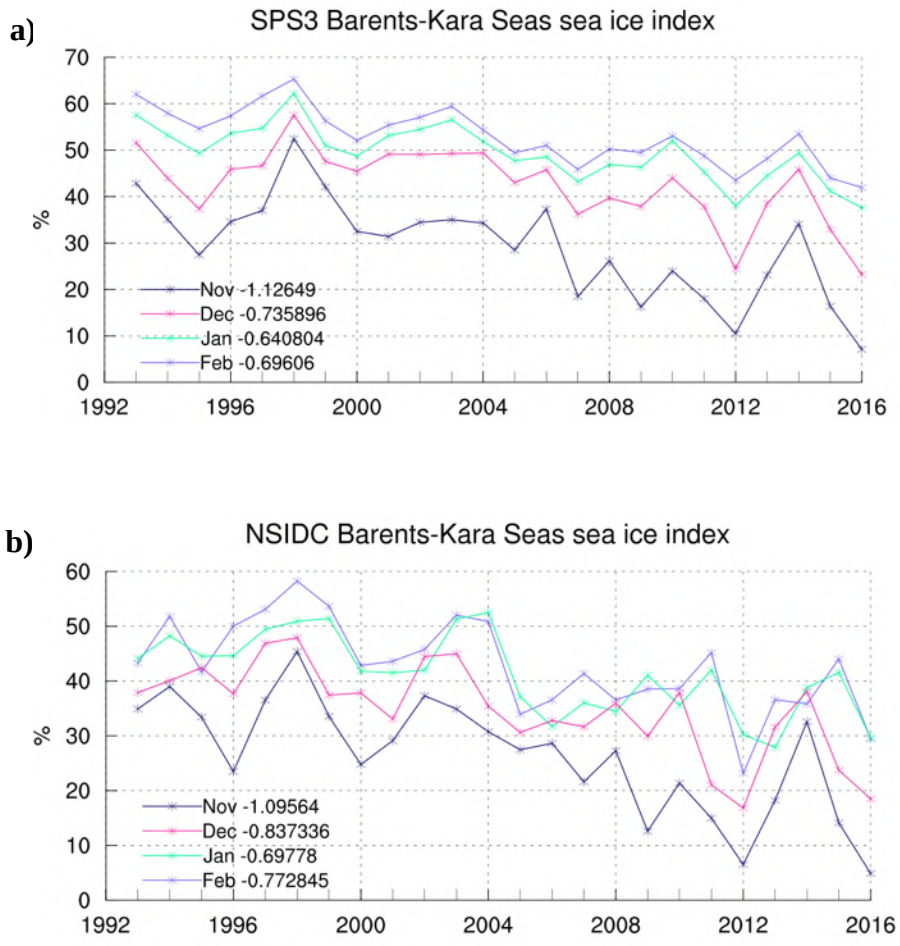

Fig. 3.4 Climatological sea ice concentration averaged over the BKS sector (15°E-90°E, 75°N-80°N) for the months November, December, January and February in SPS3 **(a)** and from observed (NSIDC) sea ice concentration **(b).**

3.1.2 Predictive skill of Arctic sea ice in CMCC-SPS3

Using a seasonal prediction system to study the impact of sea ice loss on winter atmospheric circulation, it is of interest to assess the predictive skill of Arctic sea ice concentration. Fig. 3.5 gives an overview of the predictive skill over the winter season by lead season (NDJ, DJF, JFM). In all 3 seasons, there is relatively high prediction skill for BKS sea ice with an auto-correlation coefficient (ACC) of at least 0.8 in this region, besides the Pacific side of the Arctic near the Bering Straits.

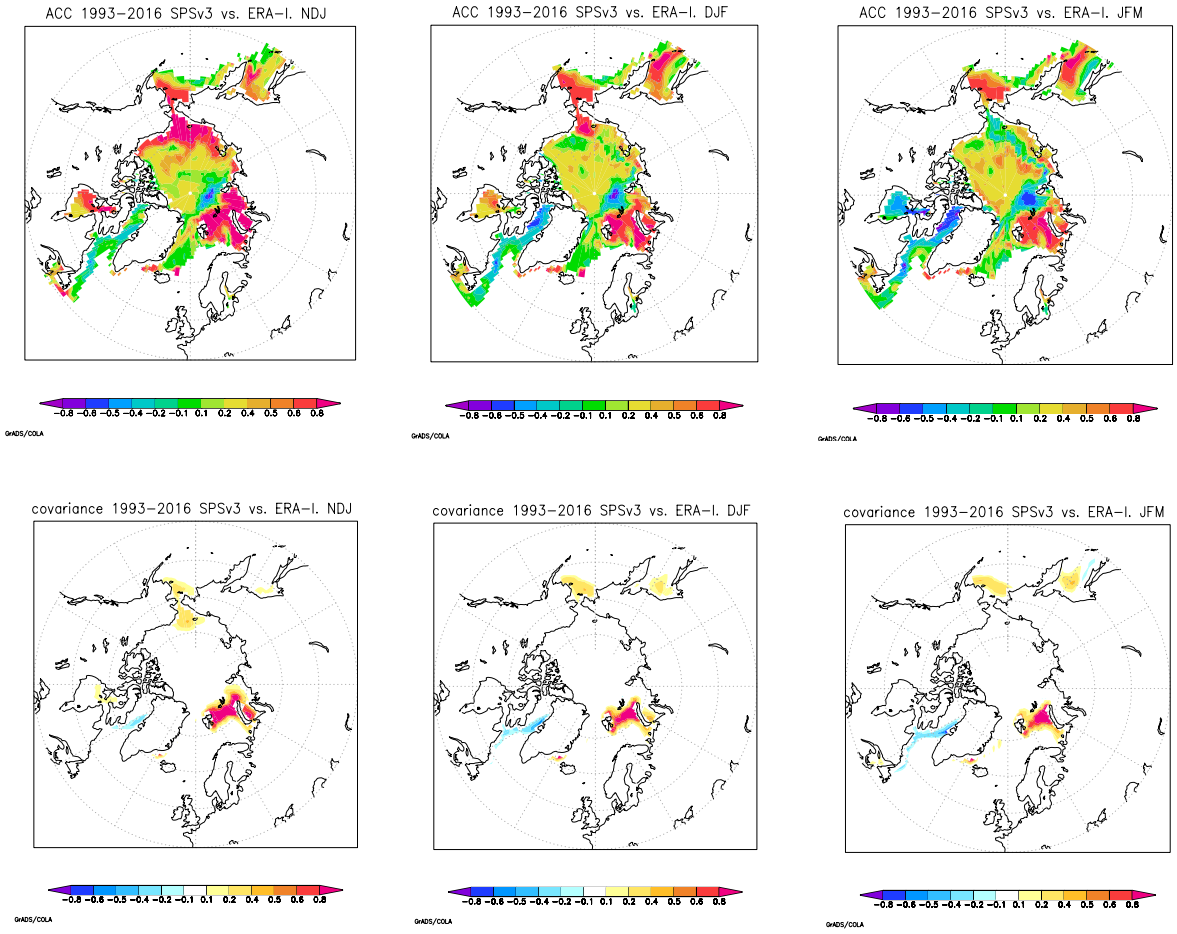

Fig. 3.5 *Upper panel:* anomaly correlation coefficient (ACC) between observed (here ERA-Interim) and simulated Arctic sea ice cover (SPS3) for NDJ, DJF and JFM (from left to right). *Lower panel*: covariance between observed and simulated sea ice cover in NDJ, DJF and JFM (from left to right).

This is supported by correspondingly high values in covariance in the BKS sector throughout the winter season with values of around 0.8 (Fig. 3.5 lower panel).

3. 1. 3 Upper-level zonal wind and geopotential height fields

The climatological zonal wind field at 250hPa over the boreal winter season (DJF) mainly reveals the subtropical jet stream (Fig. 3.6, upper panel) while the eddy-driven jet is less distinct at this level (e.g. off the east coast of North America and around 40°N). A significant positive bias is evident over the central North Pacific and over the eastern part of the mid-latitude North Atlantic and Western Europe indicating overall stronger westerlies in the model. The observed interannual variability exhibits maxima in the North Pacific and North Atlantic sectors as found in previous studies (e.g. Athanasiadis et al., 2010), while the model under-represents variability in the eastern North Atlantic sector, a bias that is common to other models and is known to relate to an under-representation of blocking (e.g. Athanasiadis et al., 2014). In the northern hemisphere, both model and observations show a double-peak in the meridional profile of the zonal wind averaged over the Atlantic sector (Fig. 3.6, left panels) and a single peak in the respective profile for the Pacific sector, however the model exhibits stronger westerlies at around circa 40°N. The winter mean maximum around 60°N in the eastern Atlantic sector is overestimated by circa 10 m s^{-1} by the model indicating an eddy-driven jet that is more zonal and extends more to the east than the one observed. Arguably, the same can be expected for the associated storm tracks. These biases can be understood in view of a underrepresentation of blocking in that sector (Sanna et al., 2017)

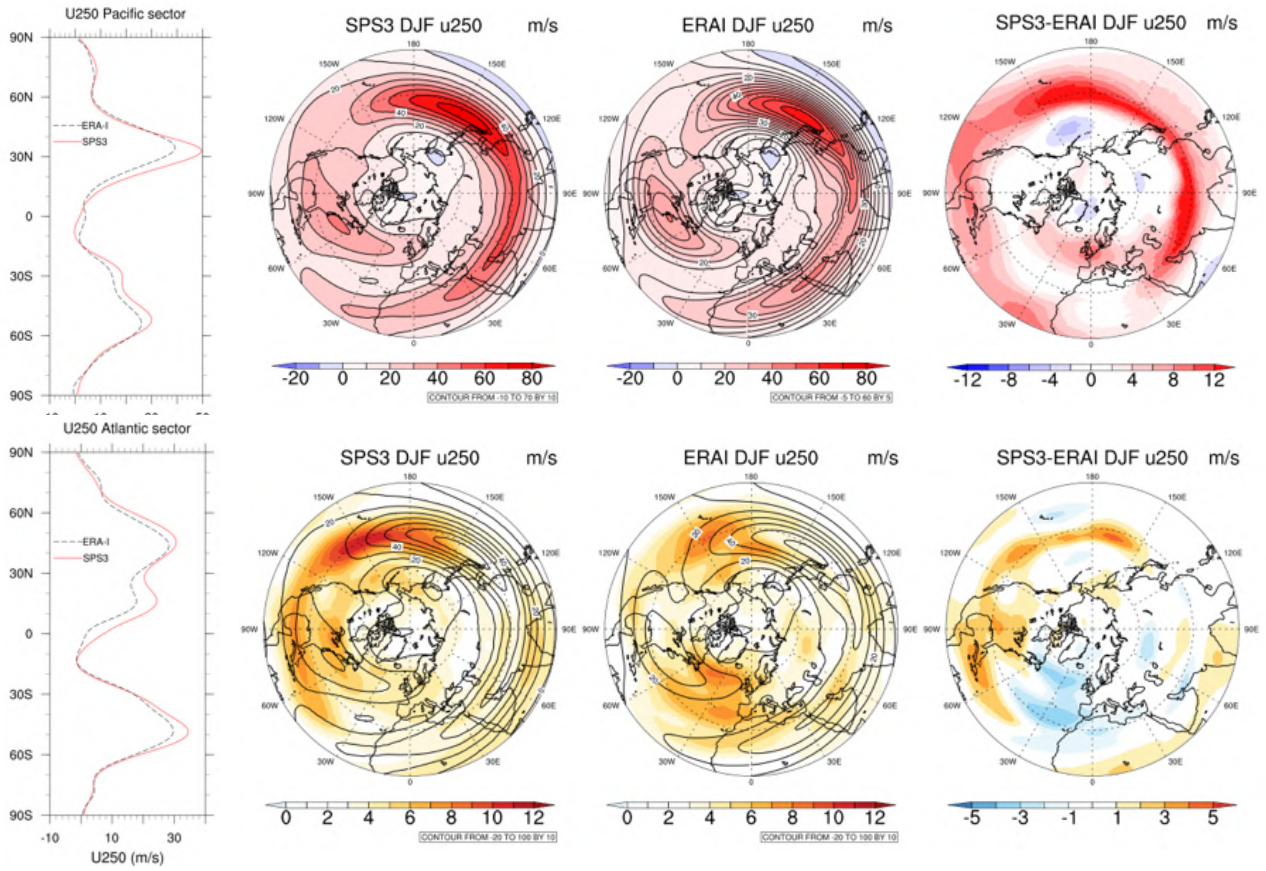

Fig. 3.6 Simulated and observed winter mean (DJF) zonal winds at 250hPa. *Upper panel:* climatology, *lower panel:* standard deviation. For reference, the contours show the DJF mean climatology. The observed wind fields are taken from the ERA-Interim reanalysis product.

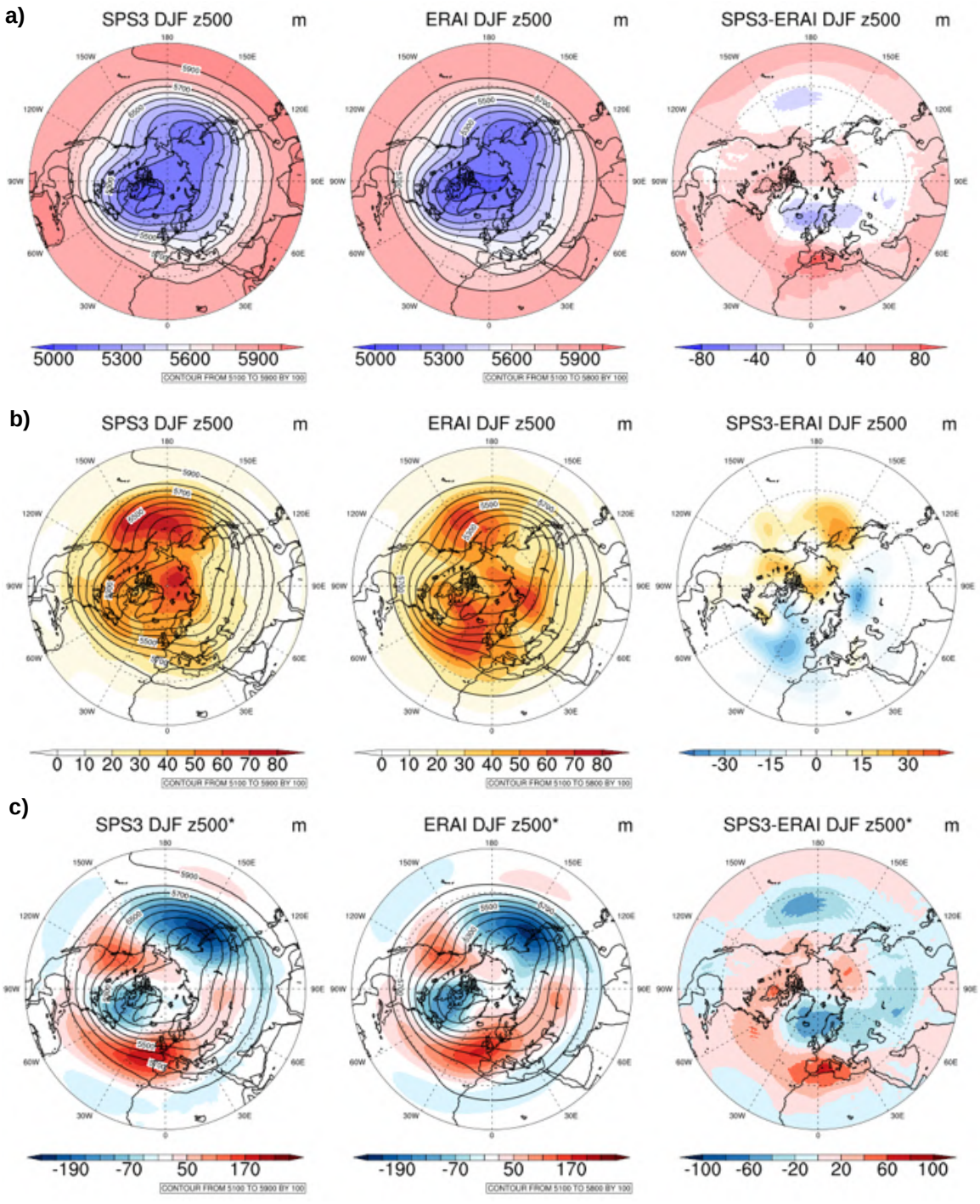

Fig. 3.7 Simulated and observed DFJ geopotential height at the 500hPa isobaric level; ***a)*** climatology, ***b)*** interannual variability, ***c)*** Z500*, where the star denotes the deviation from the zonal mean. Data for the observed wind field is taken from the ERA-Interim re-analysis product.

Looking at the geopotential height at the 500hPa level (Fig. 3.7), both the model and observations show the dominant meridional gradient as a result of the equatorward temperature gradient. Also, the typical stationary eddies are evident (zonal wave-number 1 pattern) in both the observed and the model climatology. The stationary wave field (Fig. 3.67 c) appears similar between the model and observations in terms of location and magnitude, yet there are significant positive and negative biases located over southwest Europe and the northern North Atlantic, respectively. Regarding the representation of the interannual variability of this field (Fig. 3.7 b), the latter is directly linked to the previously discussed zonal wind variability and it also reveals significant biases in the North Atlantic sector, arguably associated to an under-representation of blocking frequency in this domain. However, the interannual variability in the BKS appears to be quite good in the model comparing to observations.

3.2 Insights from a composite analysis approach

This section explores the response to reduced sea ice conditions in the BKS as inferred from composite analysis approach following the description in section 2.2.3. The observationally-deduced response is described predominantly, to which the model response is compared to. The response is here displayed for the months November to February during which the predominant winter response is expected.

3. 2. 1 Near-surface impact

Contrasting low sea ice years with high sea ice years results in a large negative sea ice cover anomaly (<-40%) in the region of the BKS (Fig. 3.8a) during November, both in ERA-I and SPS3, which is consistent with the way in which the sea ice index is defined (cf. Fig. 2.3),. There is remarkable similarity between the two data sets, in terms of spatial extent of this negative anomaly but also the fact that it gradually weakens with the course of the winter season. Era-I shows some positive anomalies in

the Labrador and Chukchi Sea (November) and Greenland Sea (December- February), and the "dipole" with positive anomalies in the Greenland Sea (January, February) has been identified earlier (e.g. Magnusdottir et al., 2004).

Sea ice anomalies translate clearly to changes in surface heat fluxes (sensible and latent heat fluxes; Fig. 3.9 a, b). In areas of sea ice 'removal', that is in the northeastern Barents Sea and in the Kara Sea, there is a positive anomaly in surface heat fluxes during reduced ice conditions, i.e. strong positive, upward fluxes can reach and exceed 80 W/m^2. A weak dipole with negative anomalies south of this region can be detected. A similar feature has been described in previous studies (Ruggieri *et al.,* 2016, Sorokina *et al.,* 2016), and has been related to a positive feedback mechanism in the following way.

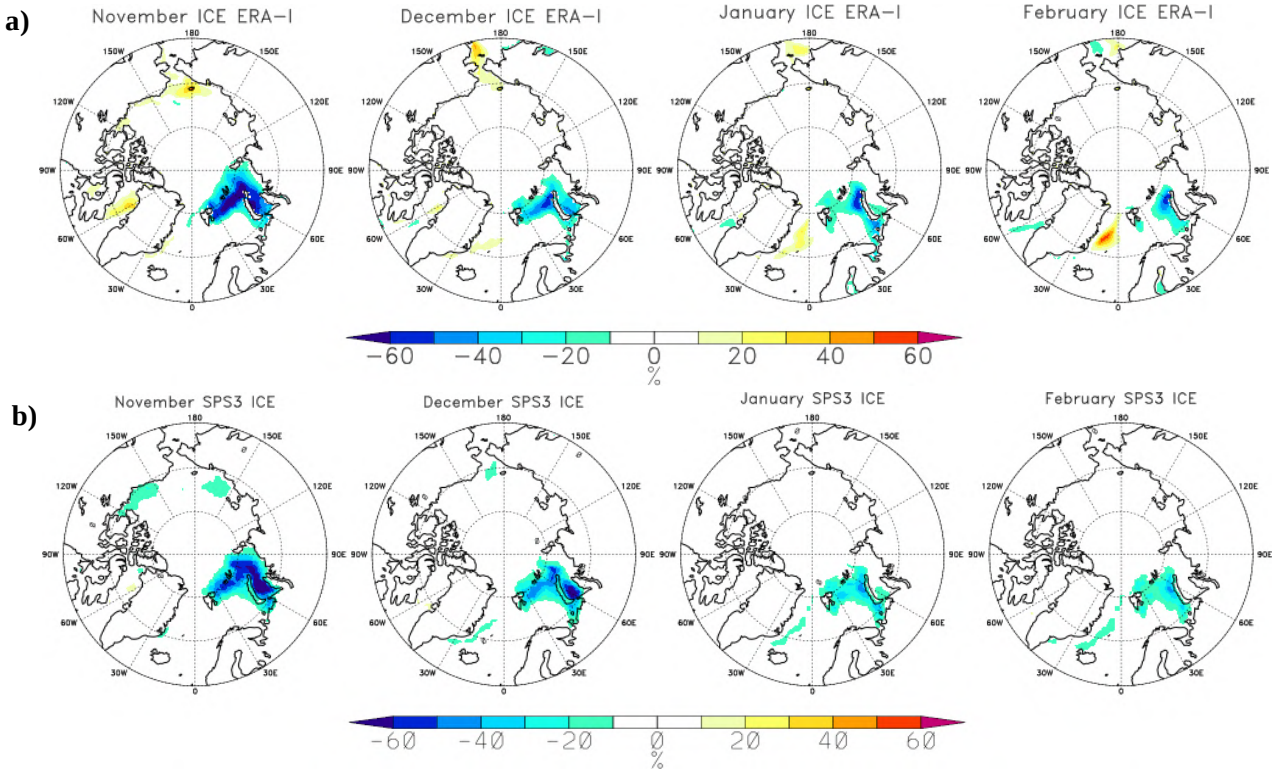

Fig. 3.8 Composite differences between LOW and HIGH sea ice years in **a)** the model (SPS3) and **b)** observations (ERA-Interim) in terms of sea ice concentration (%). Shown are the monthly means from November to February.

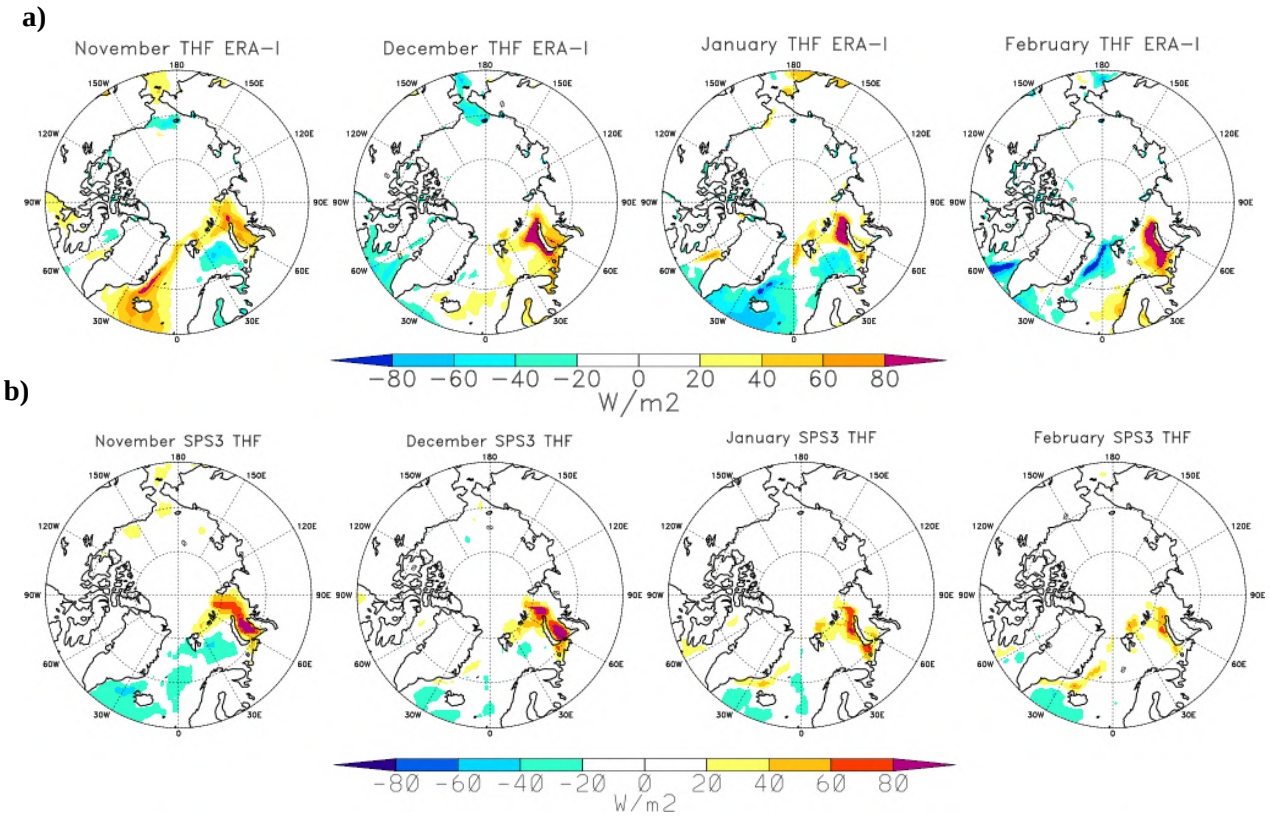

Fig. 3.9 Composite differences between LOW and HIGH sea ice years in **a)** the model (SPS3) and **b)** observations (ERA-Interim) in terms of surface turbulent heat fluxes (sensible + latent). Shown are the monthly means from November to February.

In areas of sea ice removal, a larger open ocean heating is available to the atmosphere and leads to enhanced heat fluxes from the ocean to the atmosphere. The negative anomaly south of this region can possibly be explained by southward advection of warmed air from the regions where sea ice has been removed. This feature is shared between the model and observations in November and January (observations). Apart from this region, there appear negative anomalies also elsewhere (January, northern Atlantic) and positive anomalies in the Greenland Seas (November). This likely points to other influencing factors in creating these anomalies. The model exhibits scattered positive anomalies in THF in the north Atlantic (apart from those directly to the southeast of the sea ice loss region), but no positive ones as in observations. Anomalies in surface heat fluxes readily translate into anomalies of near-surface temperature. The November response between observations and the model is

remarkably similar with a pronounced heating in the area of ice removal (and in nearby regions in the Era-I) and an indication of cooling over central/north Eurasia. This warm-Arctic-cool-continent dipole pattern has previously been described in the literature (e.g. Cohen et al., 2014). While there is a wave-like response over the polar cap visible in the observed signal with alternating cooling and warming regions, it is absent in this way in the model response. The cooling signal in the observations over central Eurasia persists over the winter and can also be seen over North America in December. The simulated response (SPS3) is comparatively weak in terms of the cooling signal, after November only the warming over the sea ice loss region remains.

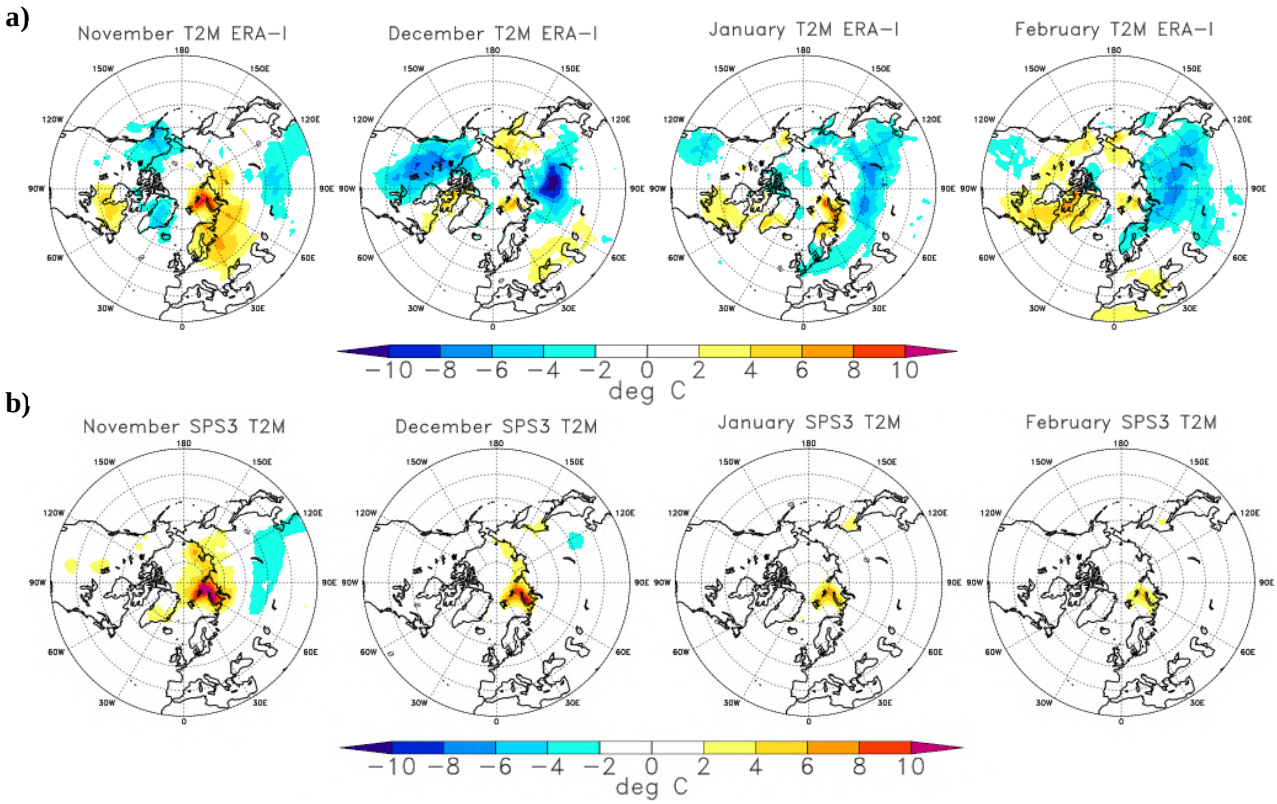

Fig. 3.10 Composite differences between LOW and HIGH sea ice years in a) observations (ERA-Interim) and b) the model (SPS3) in 2m-temperature. Shown are the monthly means from November to February.

The near-surface warming brings along increased humidity in the lower troposphere which becomes evident especially in November and December over the BKS region

together with a reduction in static stability (Fig. 3.11, Fig. 3.12). Similar to the near-surface temperature response, the pattern in both specific humidity and in static stability is less clear in observations than in the model response.

3. 2. 2 Tropospheric circulation response

Contrasting fields of mean sea level pressure reveals a pronounced signal in observations contrary to a very weak signal in the model. One feature previously described in the literature is a local low pressure anomaly over the heating area which is indicated in the observed signal but extends over the heating area, and which is not visible in the model response. The positive anomaly to the south of the BKS over Eurasia that has also been described in the literature, appears both in ERA-Interim and in the model (but in observations also over the North Pacific and the North Atlantic). There is a pronounced meridional dipole of positive and negative anomalies in the Atlantic sector in observations while there is no emergent pattern there in the model response. The simulated November response reveals a dipole with a band of positive anomalies over northeastern Eurasia and the North Atlantic and negative anomalies over the Pacific and North America.
Contrasting these patterns with what is found at the geopotential height field at 500hPa level (Fig. 3.14), it becomes apparent that mean sea level pressure fields in November seem to amplify with height into the Z500 response, i.e. being equivalent barotropic (both ERA-I and the model). The wave-like pattern that appeared in surface temperature in observations re-appears in mean sea level pressure and Z500. As in MSLP, the Z500 signal shows the prominent dipole in the Atlantic sector, again being equivalent barotropic in character. What regards the response in the model, as for sea level pressure, no prominent response can be seen after November. Hence, the observation-based signal reveals a "wavier" pattern with a distinct zonal asymmetry in geopotential height anomalies at both the 500 and MSLP pattern (Fig. 3.14).

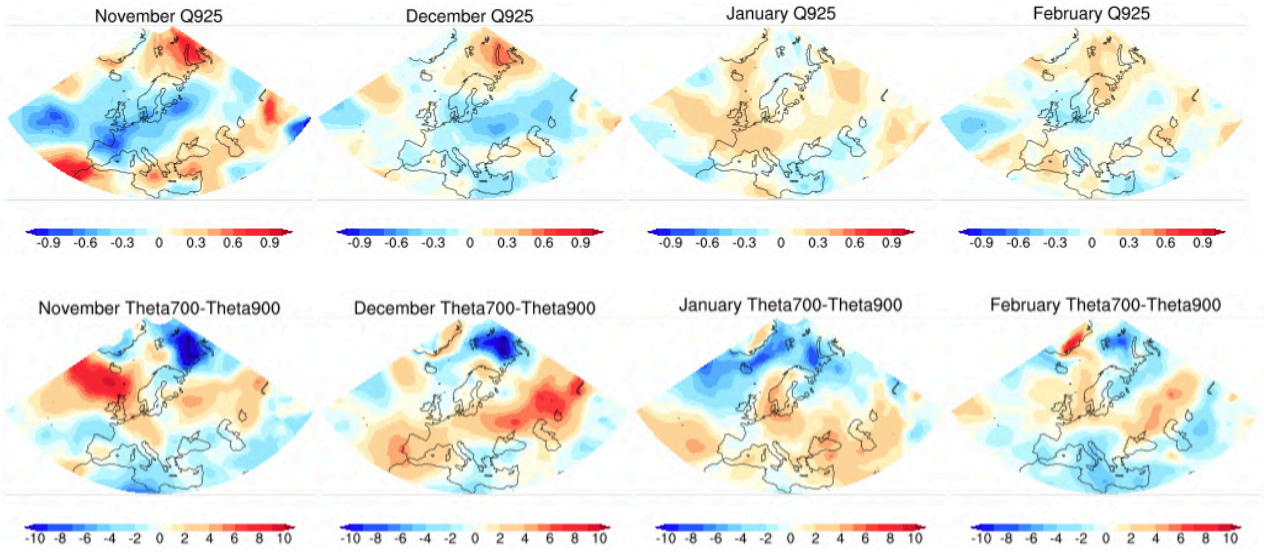

Fig. 3.11 Model composite differences between LOW and HIGH sea ice years in terms of specific humidity (g kg^{-1}; upper panel) and static stability (in K, here taken as θ_{700}-θ_{925}, lower panel). The static stability is computed as the difference in potential temperature between the 700hPa and the 900hPa level (θ_{700}-θ_{925}).

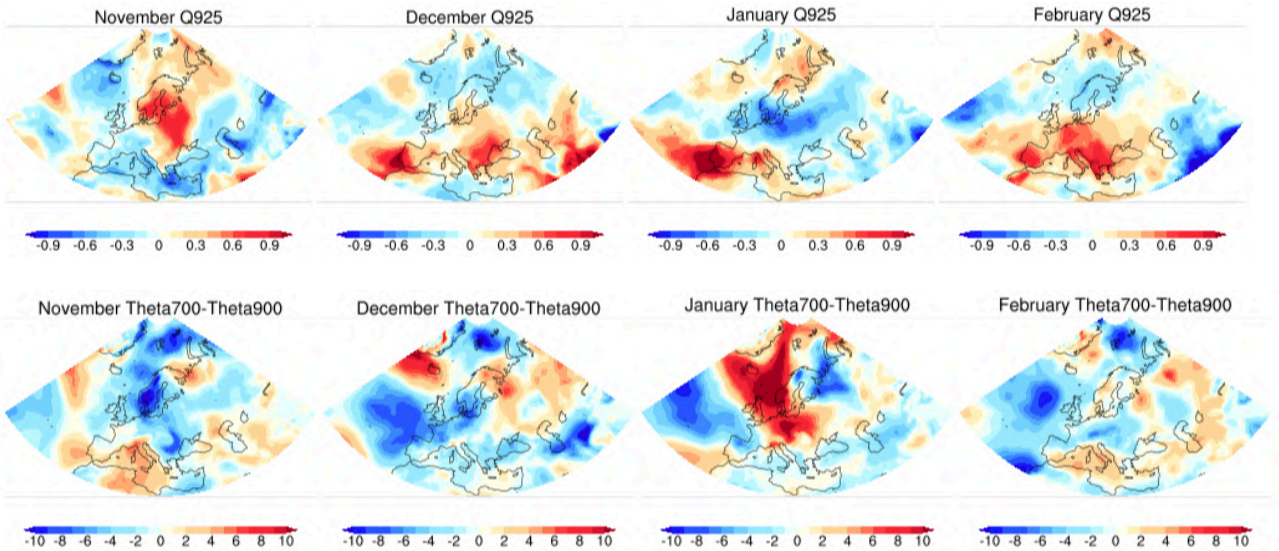

Fig. 3.12 ERA-Interim composite differences between LOW and HIGH sea ice years in terms of specific humidity (g kg^{-1}; upper panel) and static stability (in K, here computed as θ_{700}-θ_{925}, lower panel). The static stability is computed as the difference in potential temperature between the 700hPa and the 900hPa level (θ_{700}-θ_{925}).

Generally, both the model and observation-based responses reveal a predominantly barotropic structure, that is low and high pressure anomalies tend to amplify with height. This has been demonstrated also in a composite analysis study (Jaiser et al., 2012) while in contrast, a particular set of sensitivity experiment studies adopting a repeated seasonal cycle of negative sea ice anomalies (Deser et al., 2010) did not reveal a barotropic structure but instead a baroclinic vertical structure with negative anomalies in geopotential height in the lower troposphere (1000hPa) and positive anomalies at upper levels (500hPa). Obviously, such an experimental set-up differs from the analysis performed here (composite analysis of the model's hindcast data).

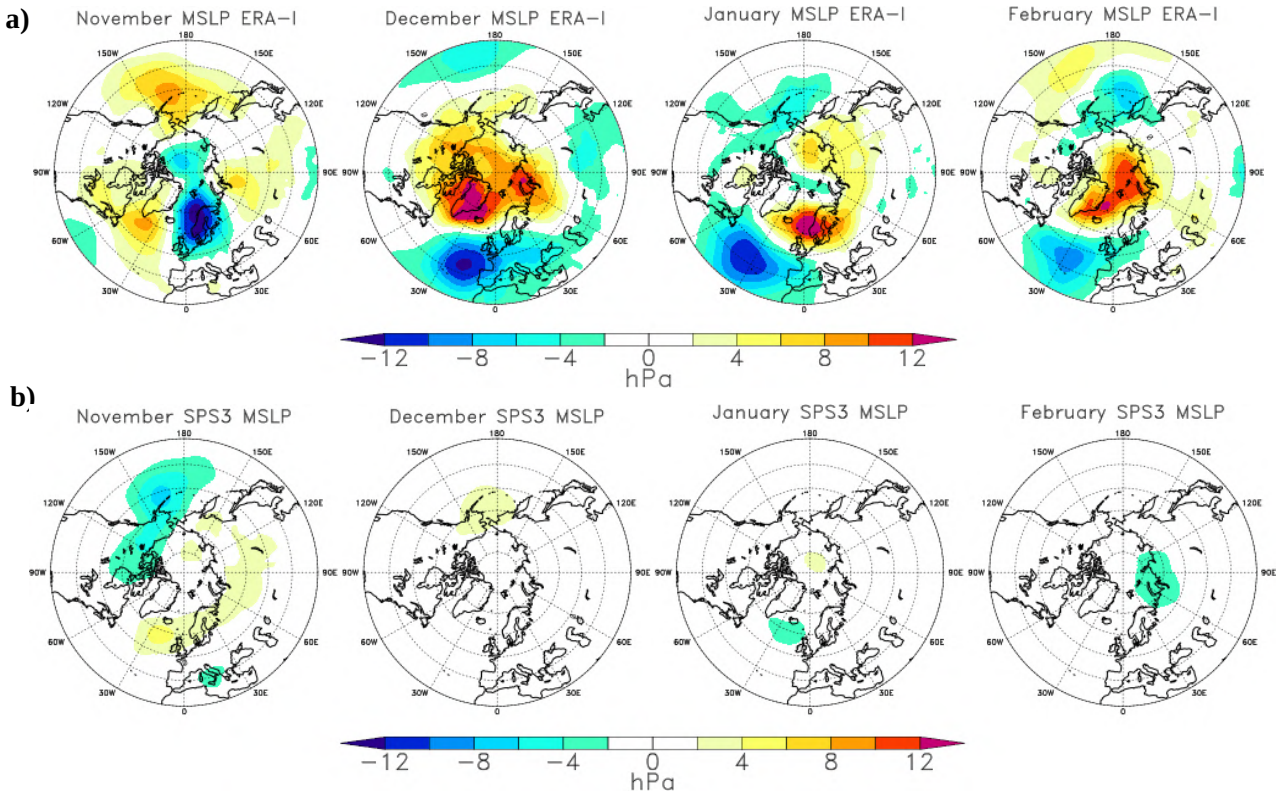

Fig. 3.13 Composite differences between LOW and HIGH sea ice years in a) ERA-Interim and b) the model (SPS3) of mean sea level pressure (hPa). Shown are the monthly means from November to February.

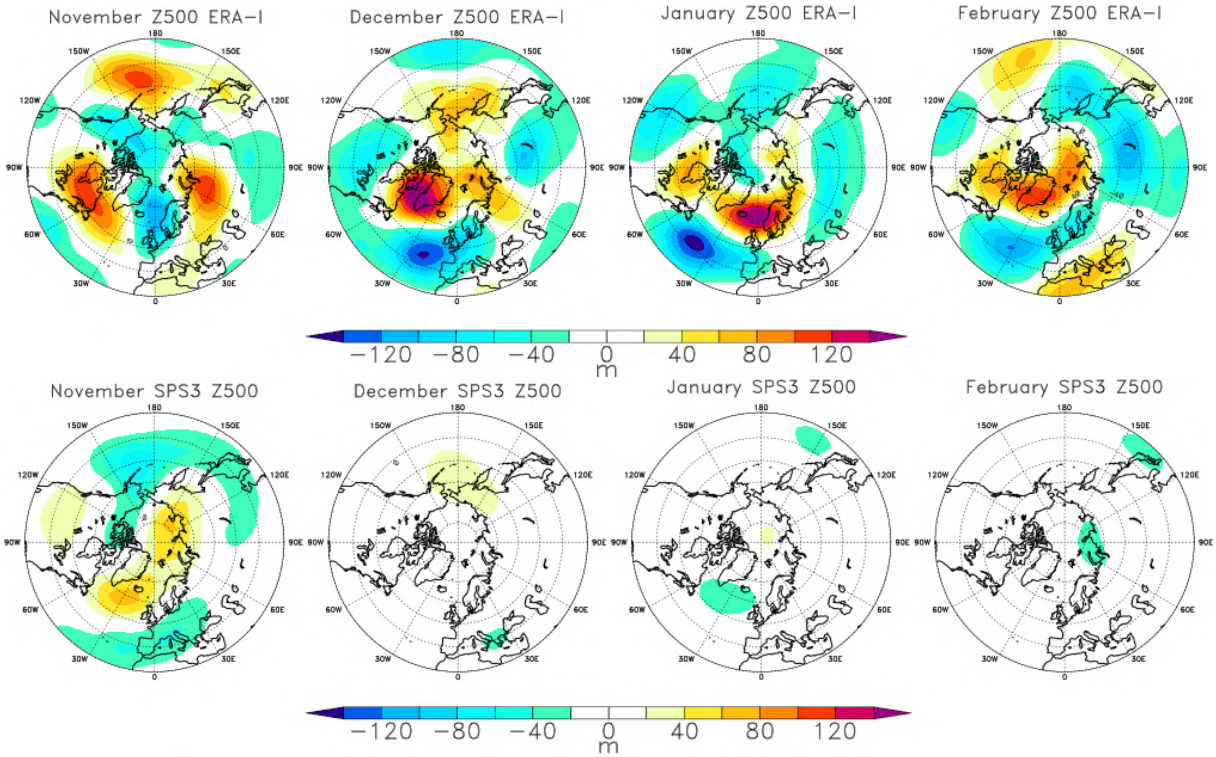

Fig. 3.14 Composite differences between LOW and HIGH sea ice years in a) ERA-Interim and b) the model (SPS3) in geopotential height at the 500hPa pressure level. Shown are the monthly means from November to February.

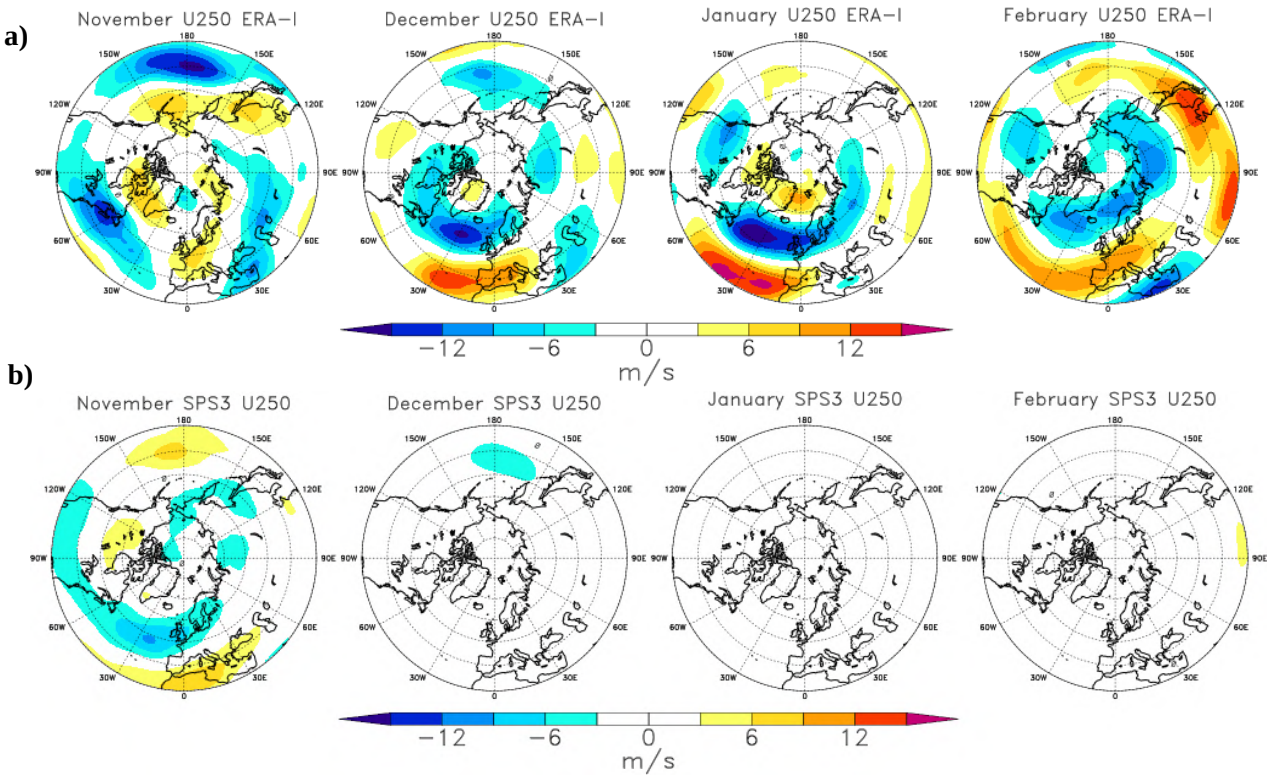

Fig. 3.15 Composite differences between LOW and HIGH sea ice years in a) ERA-Interim and b) the model (SPS3) in zonal winds at 250hPa level. Shown are the monthly means from November to February.

3. 3 Outcome from the idealized experiments with sea ice removal in the Barents-Kara Seas

3.3.1 Winter mean surface response

This section presents results from contrasting reduced sea ice conditions in November sea cover with the unperturbed control run (CTRL). The monthly mean response averaged over all winters in the hindcast period 1993-2015 of relevant surface and tropospheric fields is presented for the winter season (November-April).
Figures 3.17 – 3.22 show monthly averaged surface fields as a difference between the ice-reduced conditions and the control experiment. The imposed surface diabatic heating during November (cf. chapter 2.2) causes a pronounced and locally constrained negative sea ice difference (here onwards also termed 'anomaly') in November to the north of the Barents Sea and in all of the Kara Sea, with largest differences near the coast of Siberia. This area in fact corresponds well to the area with the largest negative trend in sea ice cover and at the same time to the area in which the surface heat fluxes show the largest inter-annual variability (Fig. 1.4). This indicates the suitability of the experimental design for studying the atmospheric response to sea ice loss in this area. The November sea ice anomaly persists well into December, being similar in terms of spatial extent, but smaller in terms of amplitude, and even slightly persists into January (northern Barents Sea). The removal or reduction of sea ice in this area leads to pronounced positive (upward) surface turbulent heat fluxes (sensible + latent heat fluxes; Fig. 3.18); with large positive anomalies off the Siberian coast in the Kara Sea (November, December), areas in which heat has been provided to the ocean by the restoring procedure. These heavy upward heat fluxes from a dipole together with negative (downward) heat fluxes, yet smaller in amplitude, in the eastern Barents Sea during (November and December). This dipole feature has been identified and described in previous work (Sorokina, 2016) and it was pointed out that this surface heat flux pattern is driven only to 2nd order by changes in sea ice cover (the 2nd EOF in Sorokina, 2016), while the major part of this response pattern can be explained by atmospheric variability (changes in low-level advection). Hence, in areas of negative surface heat fluxes (northern Barents Sea), upward heat fluxes are reduced due to the advection of warmed air from the ice loss region to the east. This is the case for

November and December when the nudging to ice-free conditions is active, while there remain only weak positive fluxes in the BKS in January.

The heavy, upward heat fluxes in the BKS during November and December cause a strong near-surface warming in the BKS (Fig. 3.20) of over 8°C (not shown). This pattern gradually fades away in terms of intensity but also spatial extent through December to January and even February. A cold anomaly develops in central Eurasia in December (however not statistically significant), while there is a widespread, statistically significant warming over all of northern Eurasia and Europe in January, and at the same time a cooling develops over North America. This cooling becomes more pronounced in February there, when also the cooling over northern Eurasia reappears. A statistically significant cooling reappears in northern Eurasia in late winter/spring (April).

3.3.2 Tropospheric circulation response

The strong diabatic heating during November causes a localized thermal low pressure anomaly over the BKS (Fig. 3.20). Then, in January, a clear dipole appears with negative anomalies in the northeast Atlantic and positive differences over the northeast Pacific sector. Together with the dipole pattern seen in Z500 in January (Fig. 3.21) over the exact same locations, this builds a deep, barotropic response and resembles a positive NAO-like circulation response. While the geopotential height anomalies reveal a dipole pattern over the northeast Pacific and North America, only a positive anomaly can be seen in sea level pressure (PSL) over the east Pacific.
As both PSL and Z500 patterns are most pronounced in January, so are the zonal winds at 250hPa over the Euro-Atlantic sector in January (Fig. 3.22). Consistent with both patterns, there is a strengthening of westerly winds seen in the northeast Atlantic around the low pressure anomaly and around the positive geopotential height anomaly and a weakening at lower latitudes which implies on a northward shift of the eddy-driven jet stream in this sector. The anomaly in the zonal winds together with the anomalies in mean sea level pressure and Z500 resemble a positive NAO-like circulation response in January.

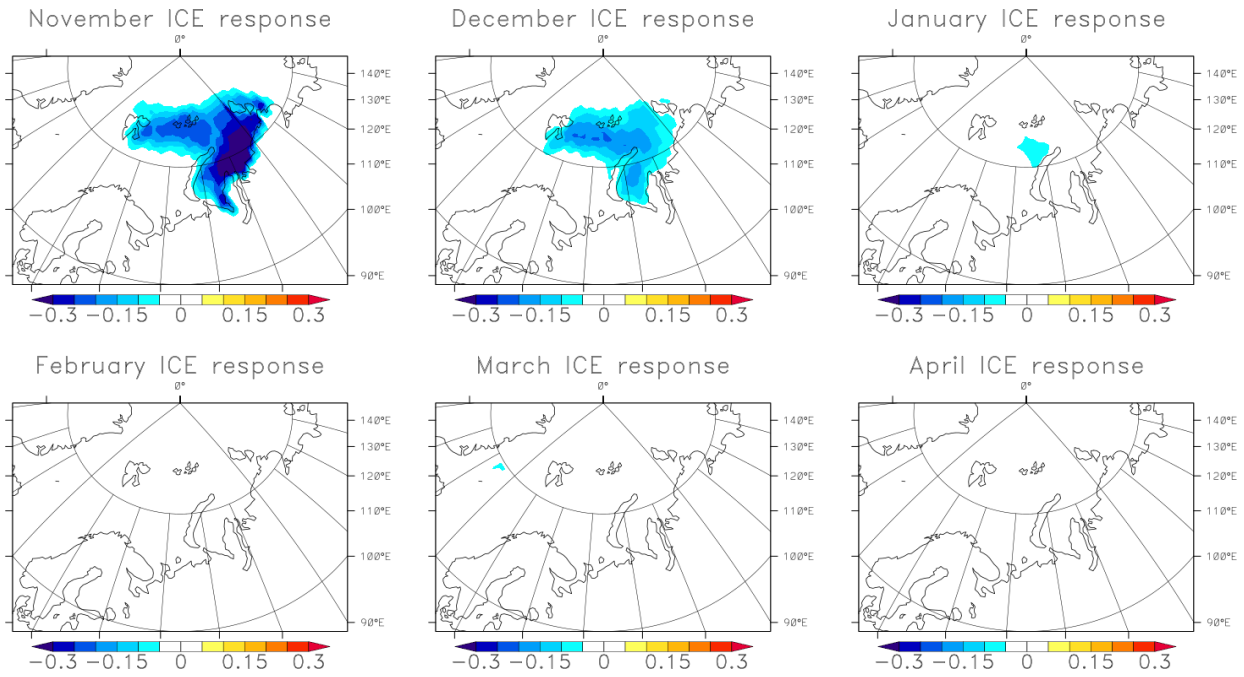

Fig. 3.17 Monthly mean difference (ICE-FREE minus CTRL) in sea ice cover (Fraction defined in the range [0, 1]), from November to April, averaged over the period 1993-2015.

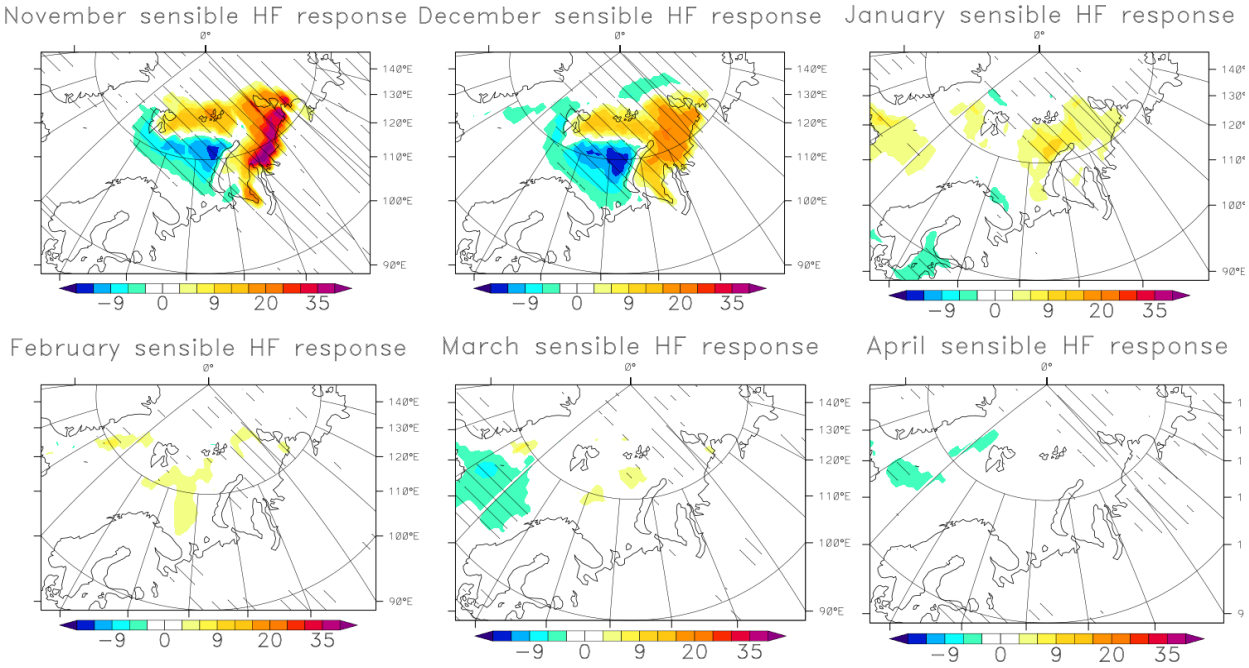

Fig. 3.18 Monthly mean difference (ice-free minus control) in surface turbulent heat fluxes (W/m^2) from November to April, averaged over the period 1993-2015. Hatched areas denote regions in which the difference between the means of the control and the perturbed experiment is significant to the 95% confidence level.

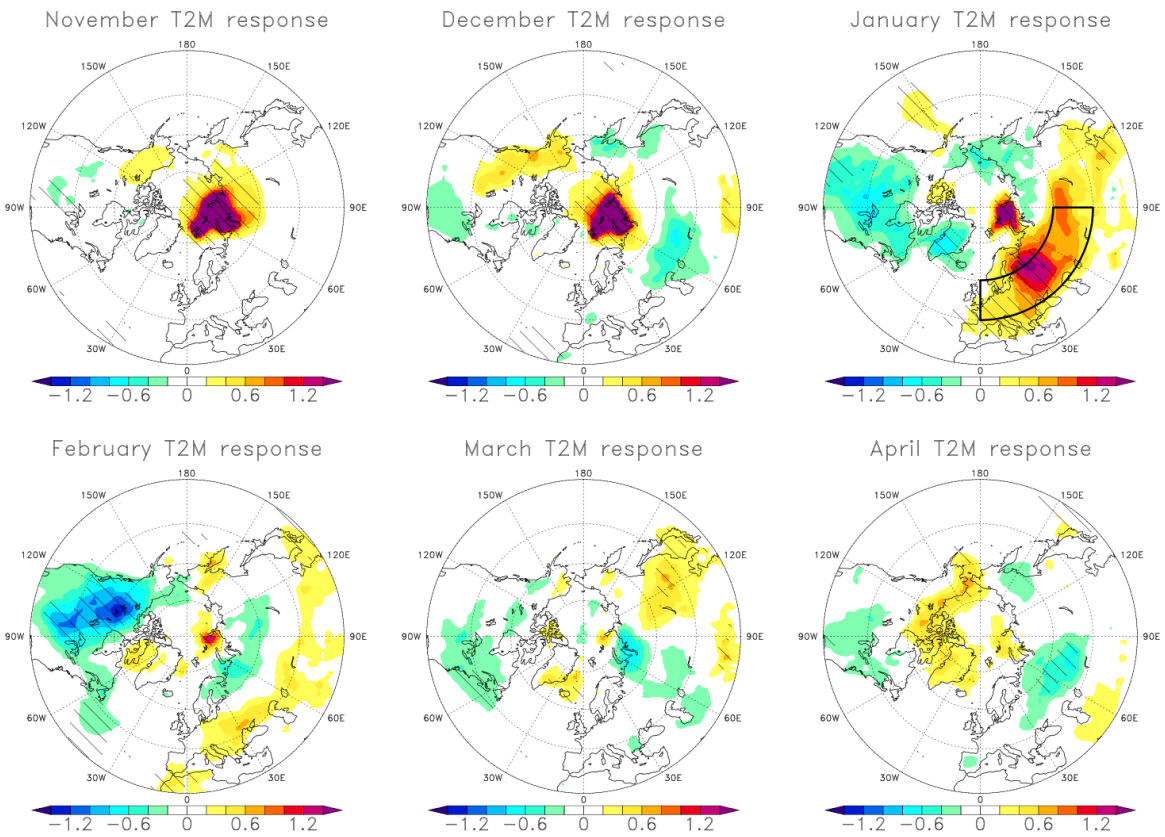

Fig. 3.19 Monthly mean difference (ice-free minus control) 2m-temperature (deg °C), from November to April, averaged over the period 1993-2015. Hatched areas denote regions in which the difference between the means of the control and the perturbed experiment is significant to the 95% confidence level.

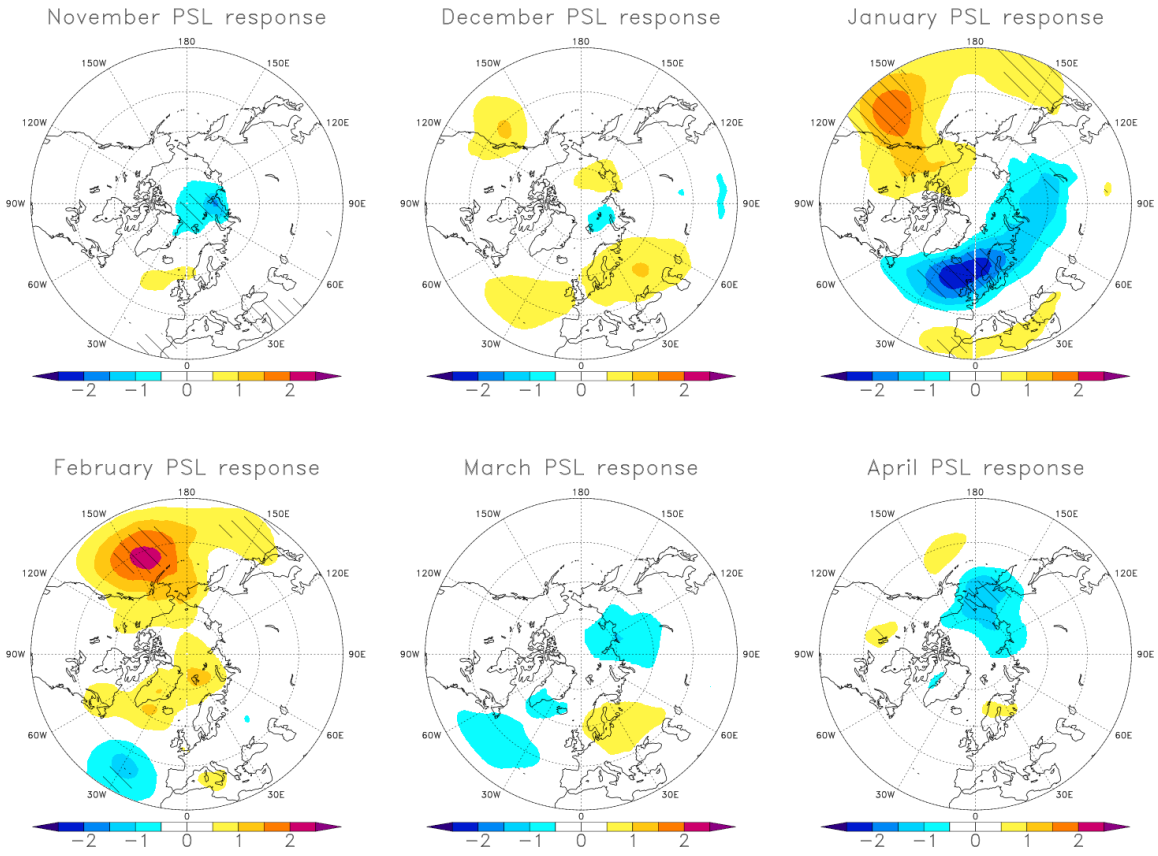

Fig. 3.20 Monthly mean difference (ICE-FREE minus CTRL) in mean sea level pressure (hPa) from November to April, averaged over the period 1993-2015. Hatched areas denote regions in which the difference between the means of the control and the perturbed experiment is significant to the 95% confidence level.

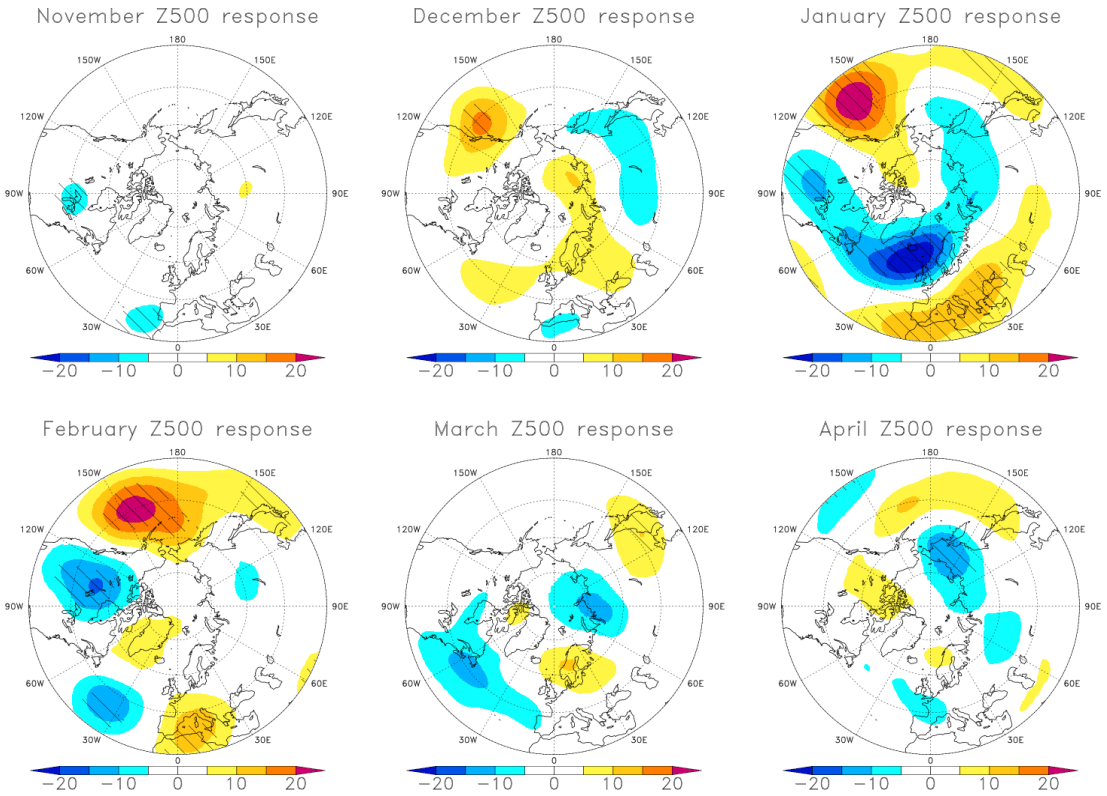

Fig. 3.21 Monthly mean difference (ice-free minus control) geopotential height at the 500hPa isobaric level (m), over the winter season from November to April, averaged over the period 1993-2015. Hatched areas denote regions in which the difference between the means of the control and the perturbed experiment is significant to the 95% confidence level.

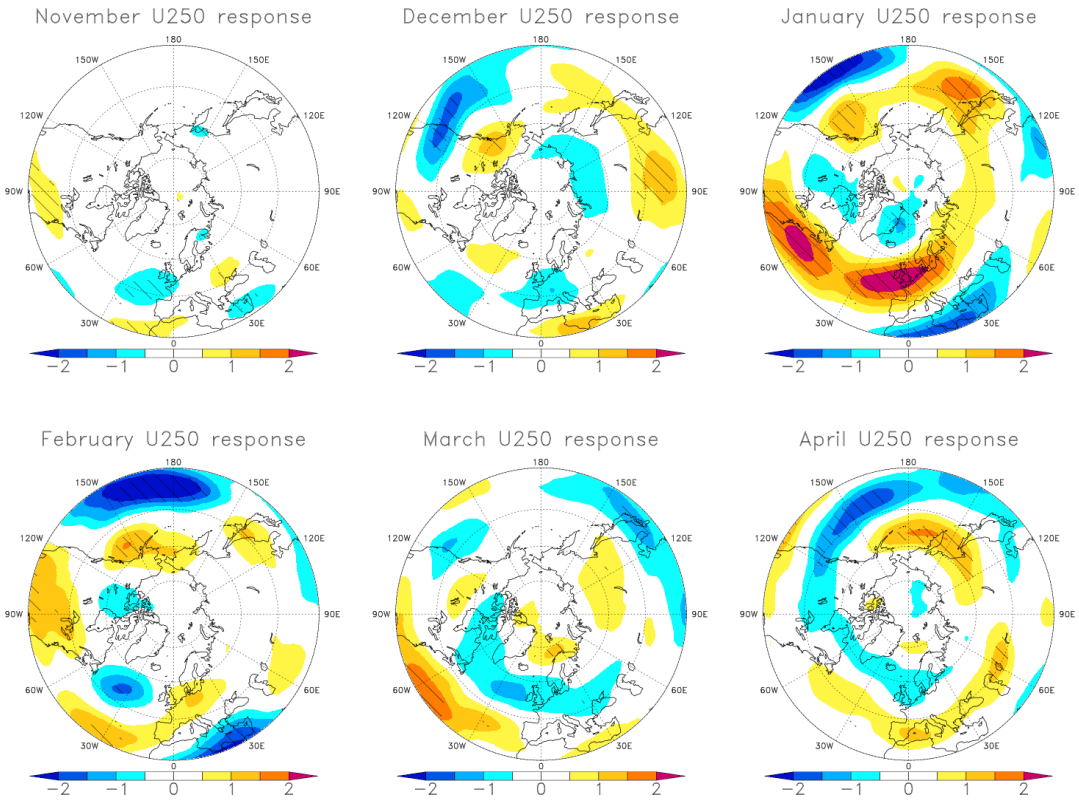

Fig. 3.22 Monthly mean difference (ice-free minus control) in the zonal wind at the 250hPa level, over the winter season from November to April, averaged over the period 1993-2015. Hatched areas denote regions in which the difference between the means of the control and the perturbed experiment is significant to the 95% confidence level.

3.3.3 Interannual variability of the response and ensemble spread

The response to sea ice reduction shown in Figures 3.17 – 3.22 shows us the mean response averaged over all years and all members. The question arises how the response to the imposed forcing varies among the years, or in other words how large the interannual variability is. Figures 3.23 and 3.24 show property indexes for each year in the period 1993 - 2015 of area-averaged fields that have appeared prominent in Figures 3.17 – 3.22. Starting from the forcing itself in the heating area (BKS), Fig. 3.23a shows the amount of sea ice removal and the near-surface temperature response for each year. It can be seen that while all years exhibit a negative sea ice cover anomaly in the BKS, as expected, the amount of sea ice removal is not unique among the years. The amount of sea ice removal in each year depends on the amount of sea ice that exists in the BKS at the beginning of the integration, i.e. at the beginning of the restoring. For each grid point, the restoring is not as efficient when ice has already built up because in this case, the restoring will tend to melt the ice by keeping SST's slightly above freezing temperature, however, since the target temperature (-1.5°C) is close to the freezing temperature (ca. -1.68°C in the Barents Sea), this melting is not very efficient. In fact, only a fraction of all years show a completely ice-free BKS in the monthly mean (not shown). The magnitude of the removal appears small (ca. 0.05-0.3) which is because the area chosen to compute the average comprises areas that are always ice-free (south of the Barents Sea).

The temperature response over the heating area is consistent with the warming seen during November (Fig. 3.19). Both sea ice cover and 2m-temperature show a clearly larger ensemble spread moving away from the initialization, the ensembles members in each year show a comparatively larger spread during December than in November (Fig. 3.23 a-d). While for sea ice, the interannual variability seems to decrease after November (in December), the interannual variability seems to increase for 2m-temperature.

The seemingly robust surface warming over Eurasia that was seen during January (Fig. 3.19) turns out to be quite variable among the single years with nearly a third of the years exhibiting a cooling in response to the sea ice loss with a generally large spread among the years (Fig. 3.24a). The interannual variability for 2m-temperature is less for an area average that show a near-zero response (Fig. 3.19, 3.24b).

The geopotential height response at 500hPa and the zonal wind response at 250hPa averaged over the northwest Atlantic during January (Fig. 3.24 c, d) show both positive as well as negative area-averaged responses, and as for the near-surface temperature the ensemble spread is relatively large. This behaviour is similar when choosing larger areas to compute the average (here shown for Z500 averaged over the polar cap >60N; Fig 3.24e-f), based on the fact even when choosing prominent regions as they appear in Fig. 3.17-3.22, the interannual spread may still be large, with some years having a positive and some years a negative ensemble mean response. For the responses shown for indexes in January and February (T2M, Z500 and U250), the ensemble spread is more than twice as large as the interannual variability. This points to the large internal variability in the atmosphere and the need for a large ensemble size.

3.3.4 Dependence on the forcing magnitude

The results of the last section indicate that the sign of the response (i.e. the ensemble mean of each year) varies from year to year. Another question to ask is whether the sign or magnitude of the response could depend on the magnitude of the forcing (the amount of sea ice removal in the BKS). Earlier studies have found a highly non-linear response to sea ice loss in the BKS; Petoukov and Semenov (2010) in their simulation with an AGCM found a transition from an anomalous cyclonic circulation to an anticyclonic circulation and back again over the eastern Arctic when reducing gradually the sea ice cover from 100% to ice-free conditions. McKenna et al. (2018) using an intermediate complexity GCM, found a negative NAO-like circulation response when using end of 21st century-projected sea ice anomalies and a positive NAO-like circulation response when using half of this forcing magnitude. In Fig. 3.25 - 3.27, it is investigated if area-averaged indexes of the response defined as in Fig. 3.23 and 3.24 depend on the amount of sea ice removal. As expected over the north Eurasian sector, there is little relation between the response and the amount of sea ice removal during November and April. The spread between the years increases with the progress of the winter season, when the remote impact of the sea ice removal starts to take effect (Fig. 3.25). There is a strong positive dependence (r=0.51) in December

between amount of sea ice removal and 2m-temperature, when only a sufficiently large removal of sea ice leads to the cooling seen that is seen in Fig. 3.19. The relationship changes sign during January, February and March when sufficiently large sea ice removal leads to warming over this area, as seen in the January response (Fig. 3.19). Even when the area-averaged response (0-90E, 45-60N) is near-zero such as during February, temperature response and the amount of sea ice removal are quite large anti-correlated (r=-0.44) which points to the large inter-annual variability. Considering a larger-scale area average, shown here for Z500 response averaged over the polar cap (north of 60N; Fig. 3.26), it can be seen that there is a positive trend for January, February, March and April (the negative trend during November and December is less considered because of the predominance of the near-surface response during these months). Hence, as the sea ice removal increases, there is an increasingly negative response in Z500 averaged over the polar cap, especially for January (r=0.41). A similar result can be seen for the zonal wind field at 250hPa over the extended Euro-Atlantic domain (strength (and position) of the Atlantic eddy-driven jet stream). Only when there is a "significantly" large sea ice removal, we see a positive anomaly in the zonal winds over the Euro-Atlantic sector, while for smaller values of the "forcing" (sea ice removal), there is a weakening of the Atlantic jet, here seen for January, February and March (Fig. 3.27), even though as for Z500, the area is extended here.

3. 3. 5 The importance of other drivers in shaping the response

It is known that Euro-Atlantic atmospheric winter circulation is sensitive to a number of drivers, such as mid-latitude SST's (Drevillon et al., 2001), continental snow cover (Cohen et al., 2014) and tropical heating anomalies. A considerable influence on winter atmospheric circulation comes from the teleconnection with tropical Pacific climate, namely with the El Nino Southern Oscillation (ENSO; e.g. Dong et al., 2000, Greatbatch et al., 2004, Toniazzo et al., 2006). Figure 3.31 shows a first-order estimate of the influence of the El Nino 3.28 index during November on different indexes of the response in the Euro-Atlantic sector to sea ice loss in the BKS. The correlation is based on the November El Nino 3.4 index with the January response of the following year over the Euro-Atlantic sector. All time series show a statistically significant

correlation according to a student's t-test (not shown), indicating that there is a hint of ENSO on the winter atmospheric response evaluated here.

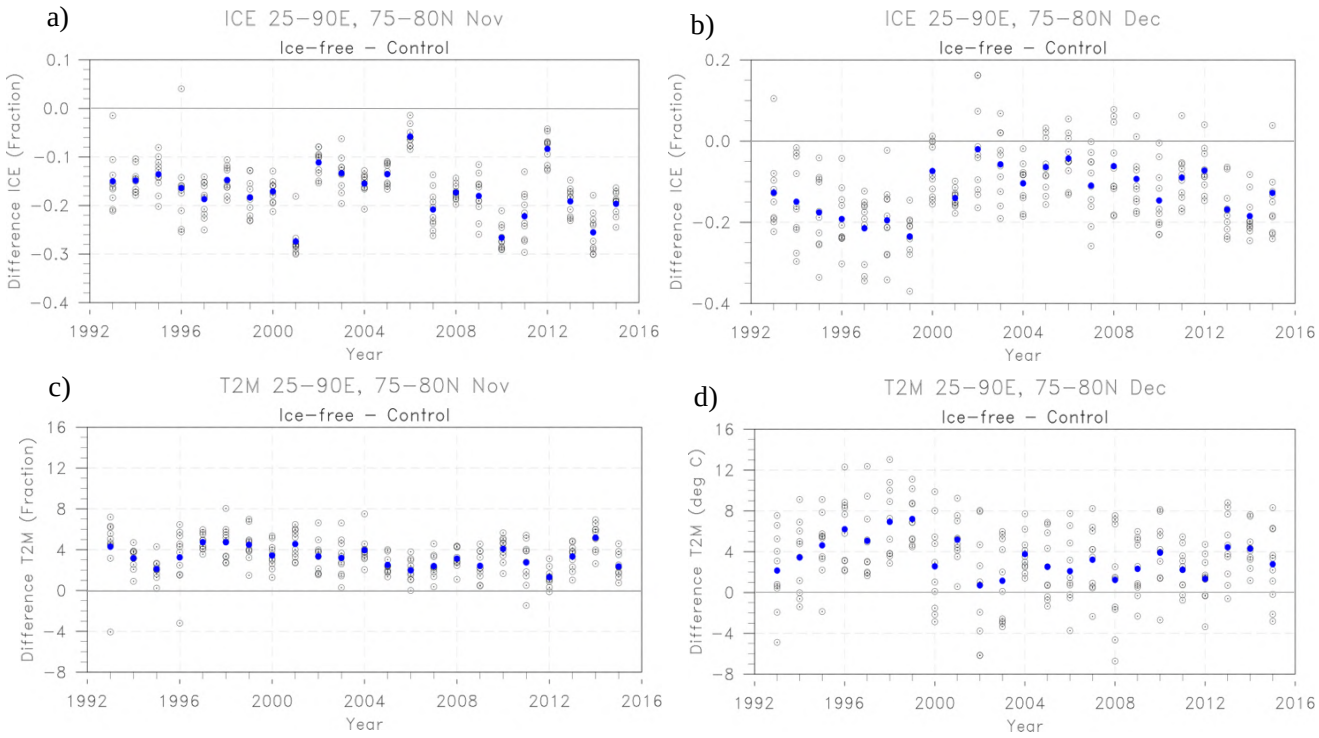

Fig. 3.23 Time series of the surface response to the imposed sea ice loss during November over the period 1993-2015. a,b) Sea ice cover, and c-f) 2m-temperature, both fields are averaged over the BKS (25-90E, 75-80N). Grey circles denote the response of single members while blue dots represent the ensemble means in each year.

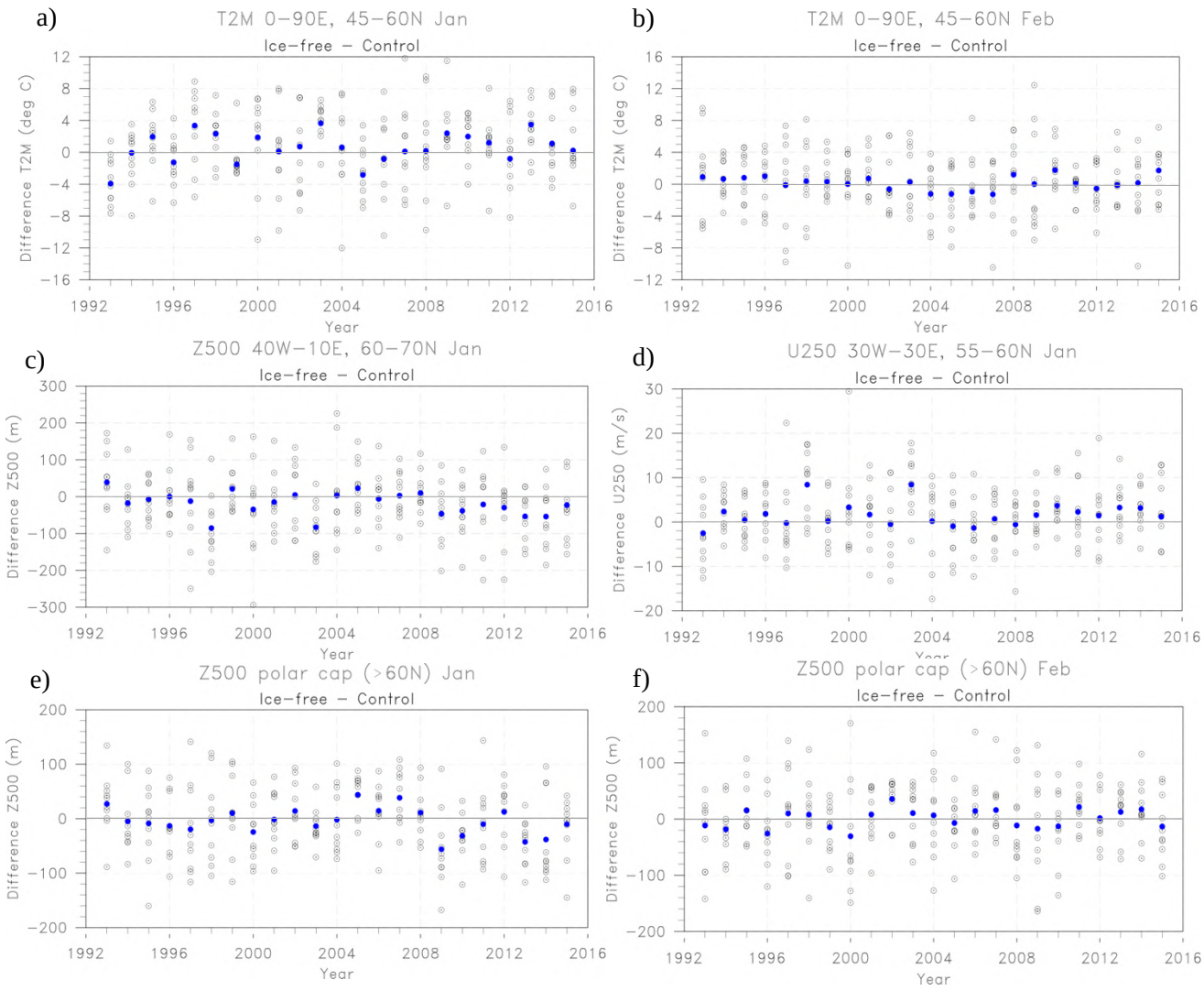

Fig. 3.24 Time series of the response to the imposed sea ice loss during November over the period 1993-2015. January (a) and February (b) 2m-temperature response over Eurasia (0-90E, 45-60N). c) and d) January geopotential height response at 500hPa in the area 40W-10E, 60-70N (c) and zonal wind response at 250hPa in the area 30W-30E, 55-60N (d). Grey circles denote the response of single members while blue dots represent the ensemble mean of each year.

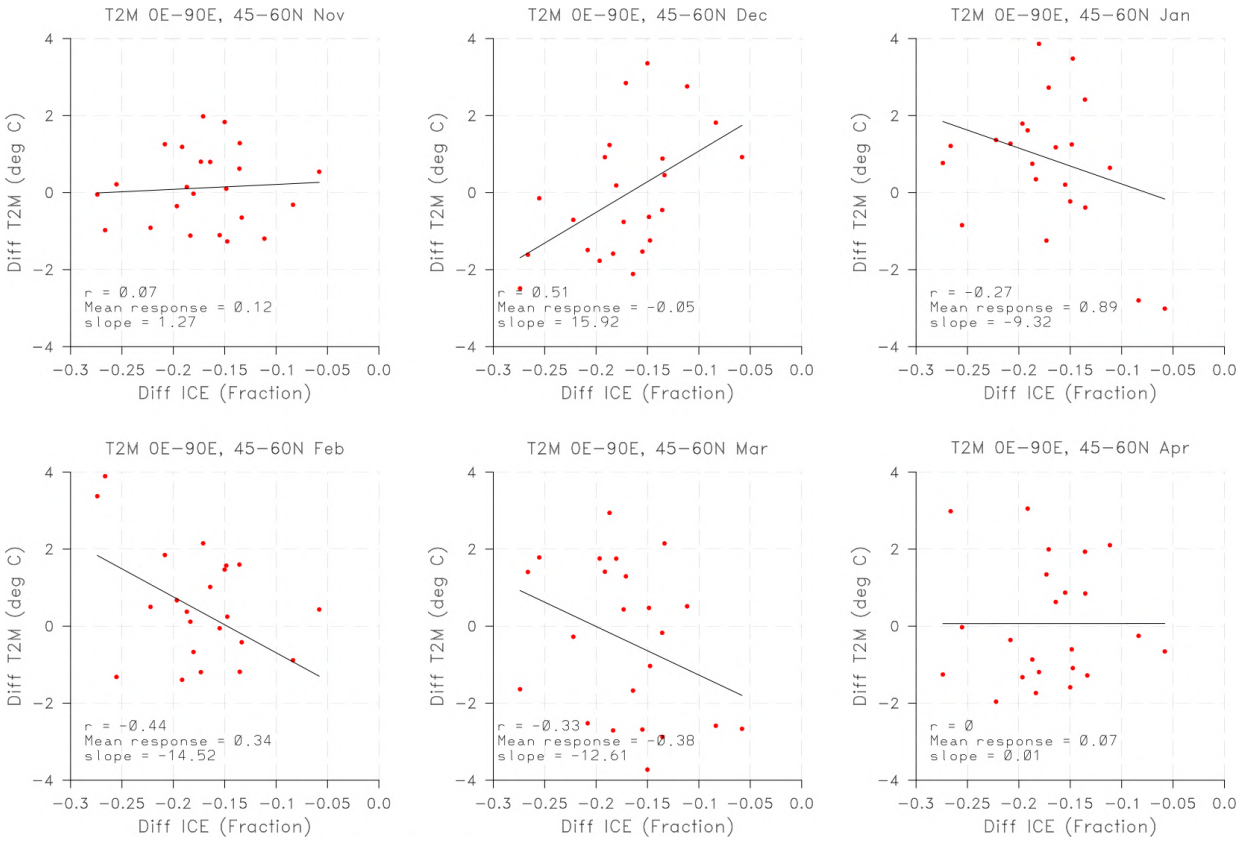

Fig. 3.25 Response of 2m-temperature response over north Eurasia (35-135°E, 50-65°N) from November (upper left) to April (lower right) as a function of sea ice removal in the BKS (25-90E, 75-80N) during November. Each dot represents the ensemble mean of each year in the period 1993-2015. The grey thin line represents the regression line. The slope of the regression line, the mean response averaged over all years and the Pearson's correlation coefficient are displayed in the bottom left corner of each plot.

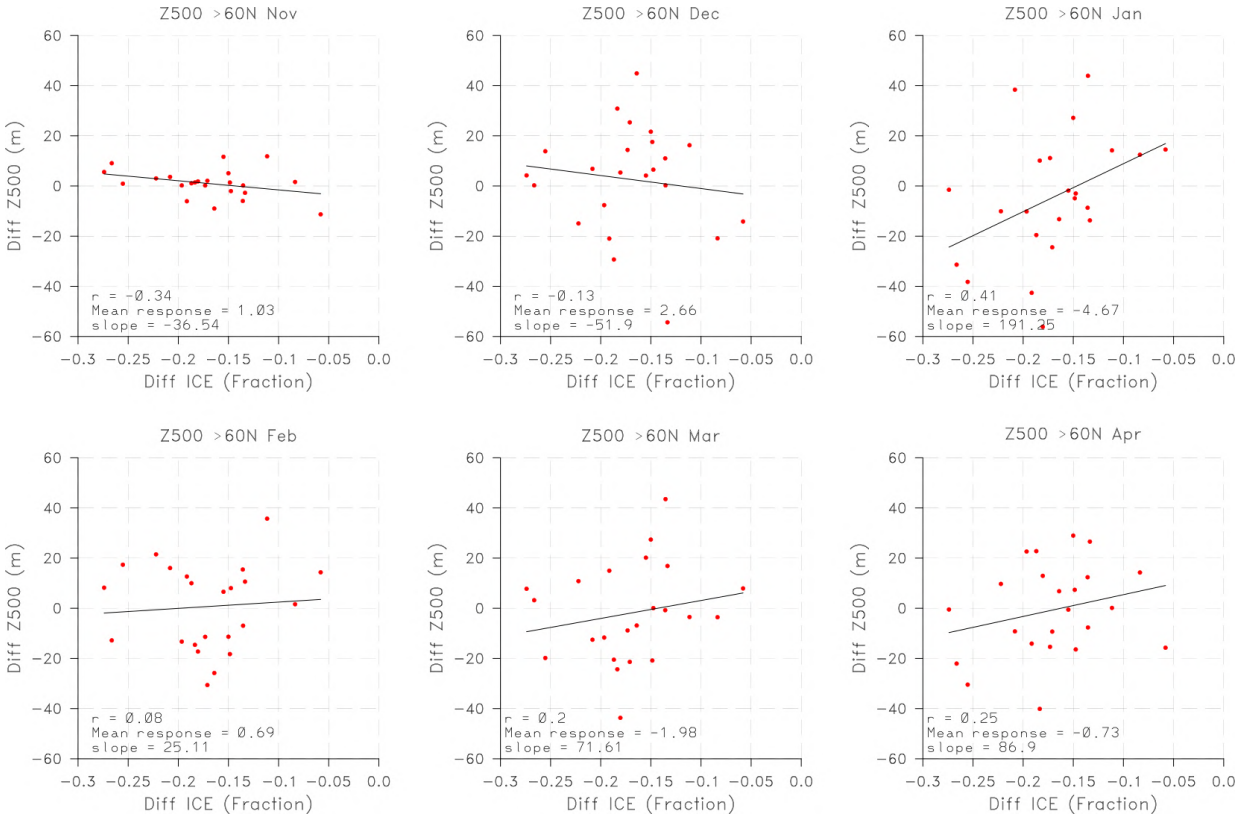

Fig. 3.26 Response of geopotential height at the 500hPa level averaged over the polar cap (>60N) as a function of sea ice removal in the BKS (25-90E, 75-80N) during November. The dots each represent the ensemble mean of each year in the period 1993-2015. The grey thin line represents the regression line. The slope of the regression line, the mean response averaged over all years and the Pearson's correlation coefficient are displayed in the bottom left corner of each plot.

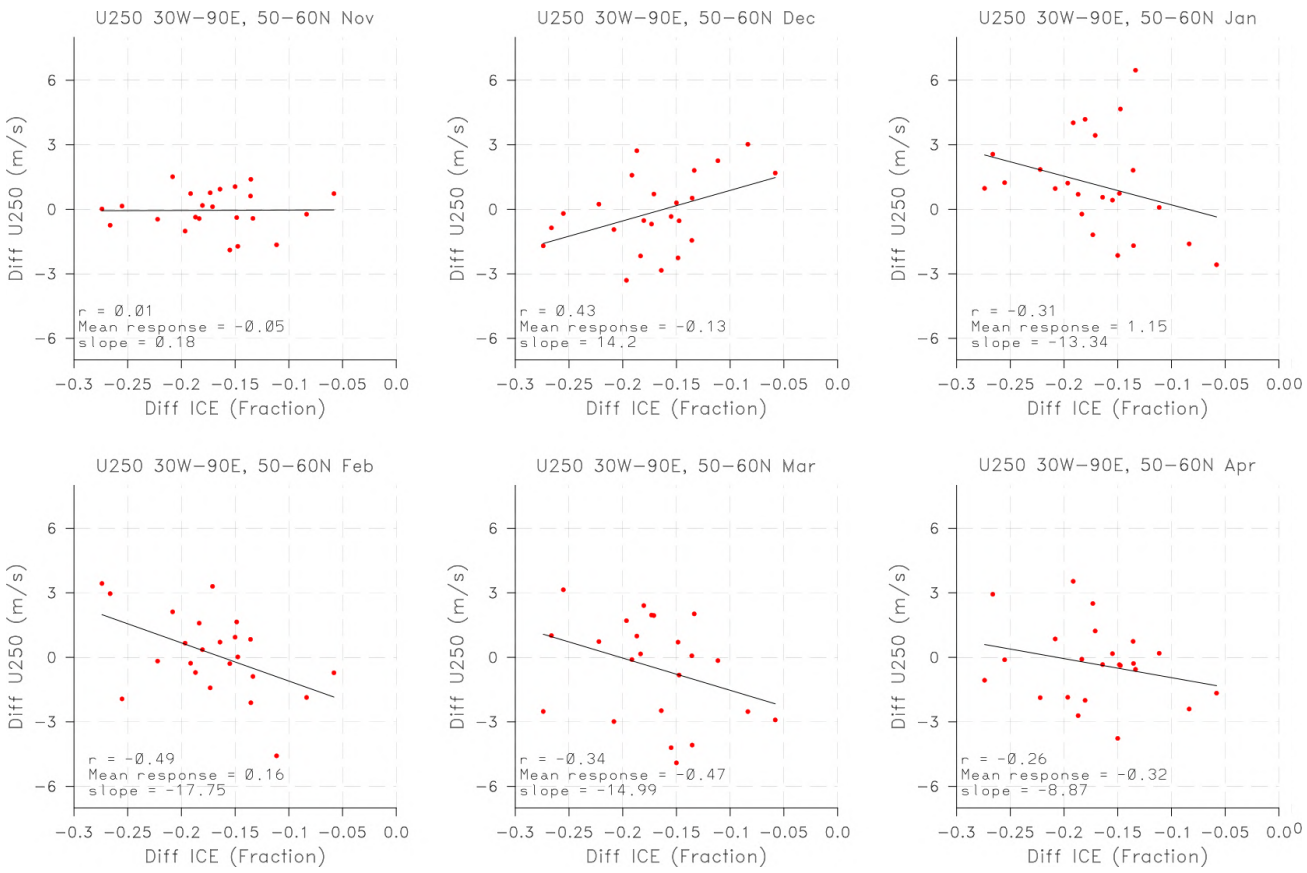

Fig. 3.27 Response of the zonal wind at the 250hPa level averaged over the Euro-Atlantic sector (30W-90E, 50-60N) as a function of sea ice removal in the BKS (25-90E, 75-80N) during November. The dots each represent the ensemble mean of each year in the period 1993-2015. The grey thin line represents the regression line. The slope of the regression line, the mean response averaged over all years and the Pearson's correlation coefficient are displayed in the bottom left corner of each plot.

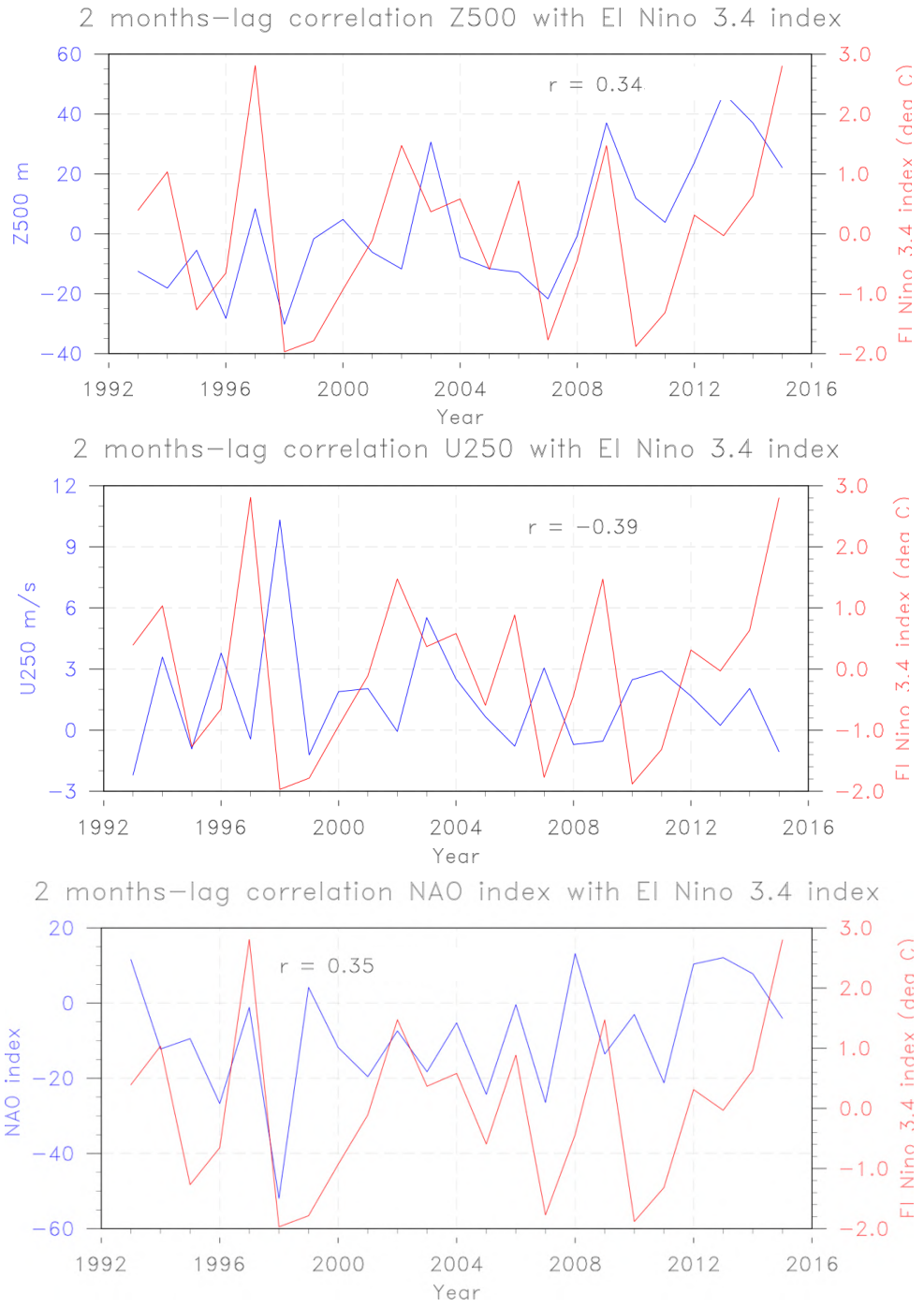

Fig. 3.28 Correlation time series response indexes over the Euro-Atlantic sector during January with the El Nino 3.4 index for the period 1993-2015. a) Z500 (averaged over 10E-30W, 60-70N; *upper panel*), U250 (averaged over 20E-30W, 50-60N; *middle panel*) and the NAO index (here computed as the difference between Z500 over 20W-50E, 45-50N and Z500 over 10W-30E, 60-70N.

4 Discussion

4.1. Model assessment and composite analysis

The first part of the results was dedicated to an assessment of the model's performance in terms of simulating the Arctic climate and some main characteristics of mid-latitude general circulation (section 3.1). Simulated Arctic sea generally shows a deficit in terms of sea ice cover over the winter season compared to observations, yet some features of the interannual variability are well represented (Fig. 3.2). As in observations, the long-term trend is likely to be imposed in the model by the radiative forcing (global warming) and the warming of the ocean initial state. Some features around the trend are also reproduced, which indicates good predictive skill for the SIC in the BKS, and as could be demonstrated in section 3.1.2 (Fig. 3.5).
The outcome of composite analysis approach of both the model hindcast control data as well the of the observational data (ERA-I) has revealed features typical for low sea ice conditions: a pronounced negative sea ice anomaly in the BKS, an associated dipole in surface heat fluxes and a localized warming over the area of sea ice removal (3.8 - 3.10). In both cases, there are surface heat flux anomalies outside the BKS sector such as to the east of Greenland during November and December (Fig. 3.9) pointing to other influencing factors and which likely can mask the effect of the BKS anomaly. Yet, this signal is not identical between model and ERA-I, such as November SHF which show negative and positive anomalies outside the 'heating region'. In nearly all fields, except sea ice, the model composite difference (based on an ensemble mean of 40 members) reveals a much weaker signal compared to observations throughout the winter season after November. This implies that the observational composite difference results from other processes irrelevant of the November BKS anomalous sea ice concentration in observations. In fact, even regarding the model, the anomalies seen especially in the upper fields (Z500, U250) but also in surface fields (MSLP, T2M) point to processes that could trigger the November sea ice anomalies in the first place, instead of being result of the November sea ice anomalies. This cause-and-effect issue has been touched on in chapter 1 and is an outstanding challenge in Arctic-midlatitude linkages. The model upper troposphere zonal winds (U250), geopotential height at

500hPa and the near-surface temperature anomalies (Fig. 3.10, 3.14, 3.15), for example, indicate a negative NAO – like pattern that could be responsible for the November sea ice anomalies that define the November sea ice index. The fact that they occur in November precludes a remote response due to sea ice removal in the BKS. In observations, on the contrary, besides revealing a much stronger response in general, there is an indication of the negative NAO-like pattern especially from December to February which could in fact possibly be a 'response' to the sea ice loss in November.

To mitigate this problem, in other words to enhance the signal-to-noise-ratio, a larger number of years is needed so as to sample different climate states which is what has been addressed in this study. For example, the composite analysis of the SPS3 model data has revealed a pronounced negative NAO-like circulation response during November over the Euro-Atlantic sector (Fig. 3.13b) while the ICE-FREE experiment revealed a positive NAO-like signal in January (Fig. 3.20-3.22) which will be discussed further below. Even if linear lagged relationships are applied in order to identify the winter response to late autumn sea ice loss in the BKS, this has previously been demonstrated to result in the opposite and false NAO response compared to sensitivity tests with reduced sea ice cover in the BKS, similar to here (Smith et al., 2017). Hence the results of the composite analysis shown in section 3.2 are given less credibility compared to the sensitivity experiment outcomes and demonstrate that Arctic mid-latitude linkages inferred from statistical relationships must be interpreted with caution.

4.2 Outcome of the sensitivity experiment with reduced sea ice cover in BKS

In contrast to the finding of the composite analysis, the idealized sensitivity experiment has revealed anomalies associated with the sea ice removal that are more distinct during the first two months of integration, i.e. a pronounced negative sea ice anomaly in the BKS and a distinct dipole anomaly in surface heat fluxes that do not show anomalies outside the heating region. This clearer signal comes about by

averaging across many years that are being forced repeatedly with the same restoring to ice-free conditions in the BKS during November. Here it is noted once again that the amount of sea ice removal is not uniform across all years (cf. Fig 3.23), the amount of sea ice being removed depends on how much sea ice there is at the beginning of the integration (beginning of the restoring procedure) and how much sea ice tends to form during the rest of November. The resulting sea ice anomaly averaged over all years that can be seen in the BKS in the sensitivity test (Fig. 3.17) corresponds well to the observed largest negative sea ice trend in this area (cf. Fig. 1.4).

The imposed heating in the BKS leads to a robust, thermodynamic response during November and December with a pronounced surface warming over the heating region (Fig. 3.19) and a development of a thermal low (Fig. 3.20). Then, in December an elongated anticyclonic anomaly forms with positive geopotential height anomalies over the eastern Arctic and north Atlantic Ocean, which leads to northerly advection of cold Arctic air over northern Eurasia (Fig. 3.21). This "warm Arctic-cold continent" pattern is a robust feature from both an observational as well as modelling point of view (e.g. Mori et al., 2014, Honda et al., 2009, Inoue et al., 2012, Nakamura et al., 2015, Kim et al., 2014) and furthermore has been identified as a negative NAO-like circulation response in these studies (as opposed to other studies which have not found this negative NAO-like response, as outlined in chapter 1). In December, the positive Z500 anomaly forms a dipole with a region of negative Z500 anomalies over eastern Eurasia (Fig. 3.21), this dipole pattern being remarkably similar to results of previous AGCM studies investigating the response to BKS sea ice loss (e.g. Inoue et al., 2012, Honda et al., 2009). This dipole structure has been suggested to arise due to a stationary Rossby wave train that is triggered by the anomalous diabatic heating in November in the BKS and that propagates south-eastwards, forming anticyclonic anomalies over the western BKS and cyclonic anomalies over central/eastern Eurasia. It has been furthermore hypothesized that this anomalous wave activity is in constructive interference with the climatological wave pattern, causing amplified meridional heat fluxes and hence an enhanced injection of tropospheric wave activity into the stratosphere, weakening the stratospheric polar vortex (e.g. Garcia-Serrano et al., 2015, Nakamura et al., 2016, Kim et al., 2014; section 1.1.3).

Progressing in the winter season, during January and February, sea level pressure and geopotential height anomalies imply a deep, equivalent barotropic circulation response that resembles the positive phase of the North Atlantic Oscillation (NAO). This is also consistent the zonal winds at the 250hPa level which show a strengthening at the poleward flank and a weakening at the equatorward flank, resulting in a poleward shift on the Euro-Atlantic jet (Fig. 3.22). This northward shift of the jet is consistent with warmer conditions over western and central Eurasia (Fig. 3.19) typical for positive NAO-like circulation phase. Hence, while this finding is consistent with itself during January, and a number of modelling studies that have found a positive NAO-like circulation response, for example in response to sea ice loss in prominent minimum years such as 2007/08 (Orsolini et al., 2012, Cassano et al., 2014, Strey et al., 2012), or with future-projected sea ice loss (Singarayer et al., 2006) or re-analysis data (King et al., 2015), it is inconsistent with the picture that emerges in terms of dynamics until December in this study, that is anticyclonic anomalies, i.e. the strengthening of the Siberian high has been found as precursor of a negative NAO-like circulation response through the mechanism described above. Hence, there seems to "switch" in processes that separate that dynamics that act up until December (thermodynamically dominating response) with those that are inferred in January and February (which are expected to be dominated by dynamical processes). One possible explanation for this apparent "switch" is considering a model- and therefore state-dependent response to eastern Arctic sea ice loss that has been stressed several times in the literature (and that is here expected to become important with a 1-month lag to the imposed sea ice loss). Smith et al. (2017) in their simulations with a global climate model have demonstrated a sensitivity of the NAO-phase sign in response to Arctic sea ice loss depending on the climatological background state, in particular, the climatological background refractive index that determines the propagation of planetary waves. In their simulations, Smith et al. find a reduction in upward planetary wave activity in response to eastern Arctic sea ice loss, and a hence a poleward shift of the tropospheric jet and a positive NAO, however this relationship being dependent on background refractive index. Since there is a positive bias seen in the wintertime eddy-driven Atlantic jet (Fig.3.6), it is argued here that this bias may determine the response that is seen in January, i.e. in a positive NAO with a poleward displaced jet from its climatological position.

4.3 General remarks

The response averaged over all winters of the recent hindcast period (1993-2015) has revealed a poleward shift of the Atlantic eddy-driven jet stream and consistent with this a positive NAO-like circulation pattern in January and February. It is arguable whether this response is robust (despite being statistically significant here), considering the high ensemble spread seen for area-averaged indexes (Fig. 3.23, 3.24). To this end, it is important to note that more ensemble members are needed in order to infer a robust signal against the large internal variability of the mid-latitude atmosphere and in order to be able to pin down dynamical pathways in a more confident way (the present analysis includes ten members only for each winter forecast). Therefore, the results presented here form a detailed, but primary assessment of the dynamical response that is expected to dominate from January onwards (i.e. a 1 month-lag response considering that the sea ice anomaly persists into December). Increasing the ensemble size will shed light on the robustness of the response presented and will make it more meaningful to apply more advanced diagnostics that infer, for example, about the above-mentioned constructive interference of the anomalous with the climatological wave pattern, and hence the impact also on changes in the Atlantic storm track, one of the features that have direct impact on European communities. This is an example that illustrates why realistic sea ice initial conditions are vital for seasonal forecasts of wintertime European climate.

5 Summary and conclusions

Sea ice loss in the BKS has become a recent focus of research due to its potential impact on north European and Eurasian winter climate. This work has presented an analysis based on idealized sensitivity experiments using a state-of-the-art seasonal prediction system in which sea ice has been removed in the ocean model component in a critical area of the Arctic Ocean (Barents-Kara Seas) and at a critical time of the year (November) repeatedly for a range of years of the model's hindcast period (1993-2015).

The experimental set-up overcomes some important limitations in previous studies, that is, the impact of sea ice loss on atmospheric winter circulation is assessed here for the first time across a number of years of the recent past, instead of studying the impact of sea ice loss in particular winter seasons or in a future climate. Additionally, the method implemented to achieve ice-free conditions is a noval approach to prevent sea ice formation in an ocean model of a fully-coupled set-up by combining characteristics of a flux adjustment with those of a restoring procedure. Results indicate an initial, fast, thermodynamic response to the imposed heating during November and December which transitions into larger-scale circulation anomalies with the progress of the winter season. In response to BKS sea ice loss, there develops a geopotential height dipole in December over the eastern BKS and northern Eurasia that is consistent with previous studies. By January, sea level pressure and geopotential height anomalies imply a deep, equivalent barotropic circulation response that resembles the positive phase of the North Atlantic Oscillation (NAO). This latter, rather unexpected result is suggested to be due to a positive bias in the simulated eddy-driven jet stream intensity over the Euro-Atlantic sector which has previously demonstrated to explain a switch from a negative NAO-like to a positive NAO-like circulation response in a coupled model study. This finding stresses again the significance of state- or model dependence when studying Arctic-mid-latitude linkages.

The sign of the response seems to depend to some extent on the magnitude of the forcing, as suggested by previous studies. Furthermore, there is an indication that planetary-scale teleconnections significantly influence the sea ice-induced response over the Euro-Atlantic sector, stressing that multiple drivers act in causing wintertime mid-latitude circulation anomalies. A comparison of the idealized sensitivity experiment outcome to a composite analysis approach using the same model, contrasting low with high sea ice concentration years, has confirmed that no credibility can be given to such statistically-inferred relationships.

The presented results form a primary but necessary assessment of mechanisms that connect BKS sea ice loss with large-scale atmospheric circulation changes over the Euro-Atlantic sector. An increased ensemble size is eventually needed to confidently assess the large-scale remote response, including processes that infer about troposphere-stratosphere coupling and to changes in tropospheric circulation such as storm track characteristics, features that have direct impact on European and Eurasian countries.

6 References

Årthun, M., et al. Quantifying the influence of Atlantic heat on Barents Sea ice variability and retreat. Journal of Climate 25.13 4736-4743 (2012)

Athanasiadis, P. J., Bellucci, A., Hermanson, L., Scaife, A. A., MacLachlan, C., Arribas, A., Gualdi, S. The Representation of Atmospheric Blocking and the Associated Low-Frequency Variability in Two Seasonal Prediction Systems. Journal of Climate, 27(24), 9082-9100, doi:10.1175/JCLI-D-14-00291.1 (2014)

Athanasiadis, P. J., J. M. Wallace, and J. J. Wettstein; Patterns of wintertime jet stream variability and their relation to the storm tracks. J. Atmos. Sci., 67, 1361–1381, doi:10.1175/ 2009JAS3270.1. (2010)

Bitz, C. M., and Lipscomb, W. H. A new energy-conserving sea ice model for climate study. J. Geophys. Res, 104(15), 669-15 (1999).

Blackport, Russell, Kushner, Paul. The Transient and Equilibrium Climate Response to Rapid Summertime Sea Ice Loss in CCSM4. American Meteorological Society (2016).

Caian, M., T. Koenigk, R. Döscher, and A. Devasthale. "An interannual link between Arctic sea-ice cover and the North Atlantic Oscillation." *Climate dynamics* 50, no. 1-2 (2018): 423-441.

Cassano, E. N., Cassano, J. J., Higgins, M. E., & Serreze, M. C. Atmospheric impacts of an Arctic sea ice minimum as seen in the Community Atmosphere Model. International Journal of Climatology, 34 (3), 766-779 (2014).

Cohen, J. L., Furtado, J. C., Barlow, M. A., Alexeev, V. A., & Cherry, J. E. Arctic warming, increasing snow cover and widespread boreal winter cooling. Environmental Research Letters, 7(1), 014007 (2012)

Cohen, J., Screen, J. A., Furtado, J. C., Barlow, M., Whittleston, D., Coumou, D., Jones, J. Recent Arctic amplification and extreme mid-latitude weather. Nature Geoscience, 7(9), 627 (2014).

Comiso, J. C., Parkinson, C. L., Gersten, R., & Stock, L. Accelerated decline in the Arctic sea ice cover. *Geophysical research letters*, *35*(1) (2008).

Comiso, J. C.: Large decadal decline in the Arctic multiyear ice cover. J. Clim., 25, 1176–1193 (2012)

Cvijanovic, Ivana, Ken Caldeira, and Douglas G. MacMartin. Impacts of ocean albedo alteration on Arctic sea ice restoration and Northern Hemisphere climate. Environmental Research Letters 10.4. 044020 (2015)

Croci-Maspoli, Mischa, and Huw C. Davies. "Key dynamical features of the 2005/06 European winter." *Monthly Weather Review* 137, no. 2 (2009): 664-678.

Dee, D. P., Uppala, S. M., Simmons, A. J., Berrisford, P., Poli, P., Kobayashi, S., Bechtold, P. The ERA-Interim reanalysis: Configuration and performance of the data assimilation system. *Quarterly Journal of the royal meteorological society*, *137*(656), 553-597. (2011)

Deser, C., Magnusdottir, G., Saravanan, R., & Phillips, A. The effects of North Atlantic SST and sea ice anomalies on the winter circulation in CCM3. Part II: Direct and indirect components of the response. *Journal of Climate*, *17*(5), 877-889. (2004).

Deser, C., Tomas, R., Alexander, M., & Lawrence, D. The seasonal atmospheric response to projected Arctic sea ice loss in the late twenty-first century. *Journal of Climate*, *23*(2), 333-351. (2010)

Deser, Clara, Robert A. Tomas, and Lantao Sun. The role of ocean–atmosphere coupling in the zonal-mean atmospheric response to Arctic sea ice loss. Journal of Climate 28.6 2168-2186. (2015)

Drévillon, M., L. Terray, P. Rogel, and C. Cassou. "Mid latitude Atlantic SST influence on European winter climate variability in the NCEP reanalysis." *Climate Dynamics* 18, no. 3-4 (2001): 331-344.

Dong, B. W., R. T. Sutton, S. P. Jewson, A. O'Neill, and J. M. Slingo. Predictable winter climate in the North Atlantic sector during the 1997–1999 ENSO cycle, *Geophys. Res. Lett.*, 27(7), 985–988 (2000)

Fogli, Pier Giuseppe, and D. Iovino. CMCC–CESM–NEMO: Toward the New CMCC Earth System Model. *CMCC Research Paper* 248 (2014).

Francis, J. A., Chan, W., Leathers, D. J., Miller, J. R., & Veron, D. E. Winter Northern Hemisphere weather patterns remember summer Arctic sea-ice extent. *Geophysical Research Letters*, *36*(7). (2009).

García-Serrano, J., Frankignoul, C., Gastineau, G., & De La Càmara, A. On the predictability of the winter Euro-Atlantic climate: lagged influence of autumn Arctic sea ice. *Journal of Climate*, *28*(13), 5195-5216. (2015)

García-Serrano, J., Frankignoul, C., King, M. P., Arribas, A., Gao, Y., Guemas, V., Sanchez-Gomez, E. Multi-model assessment of linkages between eastern Arctic sea-ice variability and the Euro-Atlantic atmospheric circulation in current climate. *Climate Dynamics*, *49* (7-8), 2407-2429 (2017)

Greatbatch, R. J., J. Lu, and K. A. Peterson: Nonstationary impact of ENSO on Euro-Atlantic winter climate. *Geophys. Res. Lett.*, 31, L02208, doi:10.1029/2003GL018542. (2004)

Haney, R.L. Surface thermal boundary condition for ocean circulation models. J.Phys. Oceanogr.1, 214:248. (1971)

Honda, Meiji, Jun Inoue, and Shozo Yamane. Influence of low Arctic sea-ice minima on anomalously cold Eurasian winters. *Geophysical Research Letters* 36.8 (2009)

Hu, A., Rooth, C., Bleck, R., & Deser, C. NAO influence on sea ice extent in the Eurasian coastal region. *Geophysical Research Letters, 29*(22), 10-1. (2002).

Hunke, E. C., and Dukowicz, J. K. An elastic-viscous-plastic model for sea ice dynamics. *Journal of Physical Oceanography*, 27(9), 1849-1867. (1997)

Inoue, Jun, Masatake E. Hori, and Koutarou Takaya. The role of Barents Sea ice in the wintertime cyclone track and emergence of a warm-Arctic cold-Siberian anomaly. *Journal of Climate 25*.7 2561-2568. (2012)

Jaiser, R., Dethloff, K., Handorf, D., Rinke, A., & Cohen, J. Impact of sea ice cover changes on the Northern Hemisphere atmospheric winter circulation. *Tellus A: Dynamic Meteorology and Oceanography*, *64*(1), 11595. (2012)

Jung, T, Ksper MA, Semmler, T, Serrar, S. Arctic influences on subseasonal nidlatitude prediction. *Geophys. Rese. Letters* 41: 3576:3680.

Kim, B. M., Son, S. W., Min, S. K., Jeong, J. H., Kim, S. J., Zhang, X. & Yoon, J. H. Weakening of the stratospheric polar vortex by Arctic sea-ice loss. Nature communications, 5, comms 5646. (2014)

Koenigk, T., Mikolajewicz, U., Jungclaus, J. H., & Kroll, A. Sea ice in the Barents Sea: seasonal to interannual variability and climate feedbacks in a global coupled model. *Climate dynamics*, 32(7-8), 1119-1138. (2009).

Koenigk, T., Caian, M., Nikulin, G., & Schimanke, S. Regional Arctic sea ice variations as predictor for winter climate conditions. Climate Dynamics, 46(1-2), 317-337. (2016)

Koster, R. D., Z. Guo, R. Yang, P. A. Dirmeyer, K. Mitchell, M. J. Puma, On the nature of soil moisture in land surface models. *J. Clim.,* 22, 4322–4335. (2009)

Kurtz, Nathan T., and Sinead L. Farrell. Large-scale surveys of snow depth on Arctic sea ice from Operation IceBridge. Geophysical Research Letters 38.20 (2011)

Lawrence, P.J., et al. Simulating the biogeochemical and biogeophysical impacts of transient land cover change and wood harvest in the Community Climate System Model (CCSM4) from 1850 to 2100. *Journal of Climate* 25.9: 3071-3095. (2012)

Magnusdottir, Gudrun, Clara Deser, and R. Saravanan. "The effects of North Atlantic SST and sea ice anomalies on the winter circulation in CCM3. Part I: Main features and storm track characteristics of the response." *Journal of Climate* 17.5 857-876. (2004)

Maslanik, J., Drobot, S., Fowler, C., Emery, W., & Barry, R. On the Arctic climate paradox and the continuing role of atmospheric circulation in affecting sea ice conditions. *Geophysical Research Letters*, *34*(3). (2007)

Maykut, Gary A. Energy exchange over young sea ice in the central Arctic. Journal of Geophysical Research: *Oceans* 83.C7: 3646-3658. (1978)

Nakamura, T., Yamazaki, K., Iwamoto, K., Honda, M., Miyoshi, Y., Ogawa, Y., & Ukita, J. A negative phase shift of the winter AO/NAO due to the recent Arctic sea-ice reduction in late autumn. *Journal of Geophysical Research: Atmospheres*, *120*(8), 3209-3227. (2015)

Nishii, Kazuaki, Hisashi Nakamura, and Yvan J. Orsolini. Geographical dependence observed in blocking high influence on the stratospheric variability through enhancement and suppression of upward planetary-wave propagation. *Journal of Climate* 24.24 6408-6423. (2011)

Oleson, K. W., et al. Technical description of version 4.5 of the Community Land Model (CLM). NCAR Tech. Note NCAR/TN-503+ STR. National Center for Atmospheric Research, Boulder, CO, 422 pp. doi: 10.5065/D6RR1W7M. (2013)

Orsolini, Y. J., Senan, R., Benestad, R. E., & Melsom, A. Autumn atmospheric response to the 2007 low Arctic sea ice extent in coupled ocean–atmosphere hindcasts. *Climate dynamics*, *38*(11-12), 2437-2448. (2012).

Overland, James E., and Muyin Wang. Large-scale atmospheric circulation changes are associated with the recent loss of Arctic sea ice. *Tellus A: Dynamic Meteorology and Oceanography* 62.1. 1-9. (2010).

Petrie, Ruth E., Len C. Shaffrey, and Rowan T. Sutton. Atmospheric response in summer linked to recent Arctic sea ice loss." Quarterly Journal of the Royal Meteorological Society141.691 2070-2076. (2015).

Parkinson, Claire L., and Donald J. Cavalieri. Arctic sea ice variability and trends, 1979–2006. *Journal of Geophysical Research: Oceans* 113.C7 (2008).

Porter, D.F., Cassano, J.J. and Serreze, M.C.,. Local and large-scale atmospheric responses to reduced Arctic sea ice and ocean warming in the WRF model. *Journal of Geophysical Research: Atmospheres*, *117*(D11). (2012)

Ruggieri, P., R. Buizza, and G. Visconti. On the link between Barents-Kara sea ice variability and European blocking. *Journal of Geophysical Research: Atmospheres* 121.10 5664-5679. (2016).

Ruggieri, P., Kucharski, F., Buizza, R. and Ambaum, M.H.P., 2017. The transient atmospheric response to a reduction of sea-ice cover in the Barents and Kara Seas. *Quarterly Journal of the Royal Meteorological Society*, *143*(704), pp.1632-1640.

Sanna, Antonella, Borelli, A., Athanasiadis, P., Materia, S., Storto, A., Navarra, A., Tibaldi, S., Gualdi, S., RP0285 – CMCC-SPS3: *The CMCC Seasonal Prediction System 3. CMCC Research Paper* 248 (2014).

Sato, K., Inoue, J. and Watanabe, M., 2014. Influence of the Gulf Stream on the Barents Sea ice retreat and Eurasian coldness during early winter. *Environmental Research Letters*, *9*(8), p.084009. (2014)

Screen, J. A., Deser, C., Simmonds, I., & Tomas, R. Atmospheric impacts of Arctic sea-ice loss, 1979–2009: Separating forced change from atmospheric internal variability. *Climate dynamics*, *43*(1-2), 333-344. (2014).

Screen, James A. "The missing Northern European winter cooling response to Arctic sea ice loss. *Nature communications* 8: 14603 (2017)

Seierstad, Ivar A., and Jürgen Bader. Impact of a projected future Arctic sea ice reduction on extratropical storminess and the NAO. Climate dynamics 33.7-8 937 (2009)

Serreze, Mark C., et al. The large-scale energy budget of the Arctic. *Journal of Geophysical Research: Atmospheres* 112.D11 (2007)

Singarayer, Joy S., Jonathan L. Bamber, and Paul J. Valdes. Twenty-first-century climate impacts from a declining Arctic sea ice cover. *Journal of Climate* 19.7 1109-1125 (2006)

Smith, D.M., Dunstone, N.J., Scaife, A.A., Fiedler, E.K., Copsey, D. and Hardiman, S.C., 2017. Atmospheric response to Arctic and Antarctic sea ice: The importance of ocean–atmosphere coupling and the background state. *Journal of Climate*, *30*(12), pp.4547-4565.

Stocker, Thomas F., et al. Climate Change 2013: The Physical Science Basis. Working Group I Contribution to the Fifth Assessment Report of the Intergovernmental Panel on Climate Change 2013 (2013)

Sorteberg, A., and B. Kvingedal. Atmospheric forcing on the Barents Sea winter ice extent. *J. of Climate*, 19, 4772–4784 (2006)

Storto A, Masina S, Dobricic S. Estimation and impact of non-uniform horizontal correlation length scales for Global Ocean physical analyses. *J. Atmos. Ocean. Technol.* 31: 2330-2349. (2014)

Stroeve, J. C., M. C. Serreze, M. M. Holland, J. E. Kay, J. Maslanik, and A. P. Barrett. The Arctic's rapidly shrinking sea ice cover: a research synthesis. *Climatic Change* 110(3-4): 1,005-1,027 (2012)

Stroeve, J. C., M. C. Serreze, M. M. Holland, J. E. Kay, J. Maslanik, and A. P. Barrett. 2011. The Arctic's rapidly shrinking sea ice cover: A research synthesis. *Climatic Change*, (2011)

Sun, L., Deser, C. and Tomas, R.A., Mechanisms of stratospheric and tropospheric circulation response to projected Arctic sea ice loss. *Journal of Climate*, *28*(19), pp.7824-7845. (2015)

Takaya, Koutarou, and Hisashi Nakamura. Precursory changes in planetary wave activity for midwinter surface pressure anomalies over the Arctic. Journal of the Meteorological Society of Japan. Ser. II 86.3 415-427 (2008)

Toniazzo, T., and A. A. Scaife, 2006: The influence of ENSO on winter North Atlantic climate. *Geophys. Res. Lett.*, 33, L24704, doi:10.1029/2006GL027881 (2006)

Thorndike, A. S., Rothrock, D. A., Maykut, G. A., & Colony, R. The thickness distribution of sea ice. *Journal of Geophysical Research,* 80(33): 4501-4513. (1975)

Vaughan, D. G., Comiso, J. C., Allison, I., Carrasco, J., Kaser, G., Kwok, R. & Rignot, E. Observations: cryosphere. *Climate change*, *2103*, 317-382 (2013)

Vihma, Timo. Effects of Arctic sea ice decline on weather and climate: A review. *Surveys in Geophysics* *35*.5 1175-1214 (2014)

Wu, Qigang, and Xiangdong Zhang. Observed forcing-feedback processes between Northern Hemisphere atmospheric circulation and Arctic sea ice coverage. *Journal of Geophysical Research: Atmospheres* *115*.D14 (2010)

Yang, Xiao-Yi, Xiaojun Yuan, and Mingfang Ting. Dynamical link between the Barents–Kara sea ice and the Arctic Oscillation. *Journal of Climate* 29.14 5103-5122 (2016)

Zhang, Pengfei, Yutian Wu, and Karen L. Smith. Prolonged effect of the stratospheric pathway in linking Barents–Kara Sea sea ice variability to the mid-latitude circulation in a simplified model. *Climate Dynamics* 50.1-2 527-539 (2018)